AFOSR Final Scientific Report
AFOSR 70-1588TR

THE MEASUREMENT OF SPHERE DRAG IN A RAREFIED GAS USING A MAGNETIC WIND TUNNEL BALANCE

Final Report
by

W. M. Phillips
A. G. Keel, Jr.
A. R. Kuhlthau

Research Sponsored by the U.S. Air Force, Office of Scientific Research, Office of Aerospace Research
Grant AF-AFOSR-1046-67

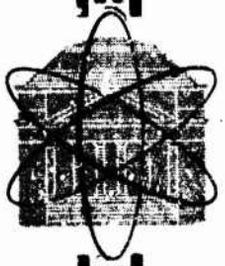

Research Laboratories for the Engineering Sciences

University of Virginia

Charlottesville

Report No. AEEP-3435-115-70U

April 1970

THE MEASUREMENT OF SPHERE DRAG IN A RAREFIED GAS USING A MAGNETIC WIND TUNNEL BALANCE

Final Report
by
W. M. Phillips
A. G. Keel, Jr.
A. R. Kuhlthau

Research Sponsored by the U.S. Air Force, Office of Scientific Research, Office of Aerospace Research
Grant AF-AFOSR-1046-67

Department of Aerospace Engineering and Engineering Physics
RESEARCH LABORATORIES FOR THE ENGINEERING SCIENCES
SCHOOL OF ENGINEERING AND APPLIED SCIENCE
UNIVERSITY OF VIRGINIA
CHARLOTTESVILLE, VIRGINIA

Report No. AEEP-3435-115-70U
April 1970

Copy No.__

ABSTRACT

Drag measurements on spheres in high speed transition regime flow are presented. The spheres are suspended electromagnetically in the low density flow field from a jet expanding freely from a small sonic nozzle into a vacuum. This arrangement provides sting-free measurements under hypersonic conditions. The current in the control coil of the electromagnetic balance is proportional to the applied force and provides a sensitive determination of the small forces encountered.

Data were taken using nitrogen and argon gases. A number of nozzle and sphere sizes were employed covering a Knudsen number range of 0.05 to 5. The results exhibit a smooth increase in the transition regime drag coefficient toward the free molecular limit for diffuse reflection and complete thermal accommodation.

Comparison is made with the available experimental results of other techniques. Improved repeatability and an extension of range of flow parameters is obtained with the present methods. The data are compared with current near-free molecular flow theories and the modified Krook solution of Willis is found to give the best agreement with the experimental results.

TABLE OF CONTENTS

LIST OF FIGURES

LIST OF SYMBOLS

SYMBOL	
A_n	Nozzle throat area (cm^2)
A_s	Sphere cross-sectional area (cm^2)
a	Sonic speed (cm/sec)
B	Magnetic (gradient) field (gauss)
C_D	Drag Coefficient
C_{DFM}	Free molecular drag coefficient
C_{DI}	High Reynolds number (invisid) drag coefficient
D	Drag force (dynes)
d_n	Nozzle throat diameter (mm)
$d_{n_{eff}}$	Effective nozzle diameter for mass flow (mm)
d_s	Sphere diameter (mm)
$\vec{dm}$	Magnetization vector of elemental volume (amp/cm)
$\vec{F}$	Sphere-magnetic field interaction force (dynes)
g	Gravitational acceleration (cm/sec^2)
Kn	Knudsen number
k	Boltzmann's constant (ergs/°K)
m	Molecular mass (gm)
m_s	Sphere mass (gm)
$\dot{m}$	Mass flow rate (gm/sec)
M	Mach number
$\overline{M}$	Molecular weight
n	Number density ($molecules/cm^2$)
P	Pressure (Torr)
P_i	Impact pressure ($dynes/cm^2$)
Re	Reynolds number
R	Gas constant (dyne-cm/gm-°K)

S	Speed ratio, $V/\sqrt{2RT}$
T	Temperature (°K)
V	Velocity (cm/sec)
X_b	Axial distance from nozzle exit to maximum free jet diameter (mm)
X_m	Axial distance from nozzle exist to Mach disc (mm)
X_s	Axial distance from nozzle exist to sphere center location (mm)
Y_b	Maximum free jet diameter (mm)
Y_m	Mach disc diameter (mm)
α	nverse Knudsen number parameter
γ	Ratio of specific heats
λ	Molecular mean free path (cm)
μ	Viscosity coefficient (dyne-sec/cm^2)
ρ	Gas density (gm/cm^3)
σ	Tangential momentum transfer coefficient
σ'	Normal momentum transfer coefficient
σ_d	Molecular diameter for hard sphere model (Å)
Ω	$\Omega^{(2,2)*}$ function of Lennard-Jones potential model

Subscripts

0	Source or stagnation conditions
1	Conditions upstream of a normal shock
2	Conditions downstream of a normal shock
∞	Free stream conditions
b	Conditions characterizing molecules reflected from a surface
c	Chamber (background) conditions
t	Theoretical (isentropic) conditions
w	Sphere wall conditions

Superscript

*	Sonic conditions

SECTION I
INTRODUCTION

The primary objective of this study is to obtain sphere drag data of improved precision in transition flow at high speeds with emphasis on near-free-molecule flow conditions. The results presented in this report were obtained using free magnetic suspension of the model in a free jet flow field. These techniques, while introducing some experimental inconveniences, eliminate two basic objections to wind tunnel testing on three dimensional models at very low density; viz. the uncertain sting or mechanical support effects, and excessive pumping requirements. In addition, the unique suspension system has a sensitivity which provides a degree of precision and reproducibility which has not heretofore been available for the measurement of the small forces encountered in low density flows.

The transition regime of gas dynamics, between continuum and free molecular flows, has been the object of much theoretical and experimental investigation in recent years.[1] Theoretical analysis of transition flow is complicated by the presence of the collision term of the Boltzmann equation. When the flow is truly free molecular some aerodynamic problems can be solved since only molecule-surface collisions are present. Even in this limiting case difficulties arise since there are unresolved questions concerning gas-surface interactions. In transition flow, intermolecular collisions, in addition to molecule-surface collisions, complicate the problem beyond mathematical comprehension unless simplifying assumptions are made. To date it has been necessary to impose severe restrictions on the analysis which delegates much responsibility to experimental results. Gross properties such as drag provide one input to the solution of transition flow problems and sphere drag measurements provide simple three dimensional aerodynamic data. The geometry is convenient, yet it provides a more realistic model for analysis than two dimensional shapes.

Satisfactory experimental data are available for two dimensional geometries in transition flow.[2,3] Problems of size and mounting in this case are such as to be readily adaptable to more conventional experimental techniques. However mechanical mounting of 3-dimensional body such as a sphere is difficult. If the body is made sufficiently large to reduce sting effects, it is difficult to achieve high Knudsen Nos over the range of high velocities which is of general practical interest. On the other hand, reducing body size leads to difficulty in meansuring the small forces which exist in low density flow.

Electromagnetic model suspension eliminates any sting or support effect and allows the accurate determination of small forces. The use of this technique has resulted in sphere drag measurements with little scatter and good reproducibility. The minimum sphere size that can be used is limited only by mechanical handling problems and the optical technique used with the support servo system. With these limitations high speed transition flow relative to the sphere can be produced.

The technique used to provide the low density flow field employs the freely expanding jet from a converging nozzle. These jets have been the object of much investigation[†] and many of their properties are known. A high velocity low density flow is produced when the gas expands into a vacuum and the core flow is isolated from the surroundings when the proper operating conditions are observed. Properties on the jet axis can be calculated with considerable confidence and a reasonable range of density and Mach number is available. The problems encountered due to the expanding nature of the flow are outweighed by the difficulty and expense of obtaining similar flow conditions by other means.

Using a combination of the magnetic suspension and free jet techniques, sphere drag measurements have been made in the range from transition flow to nearly free molecular conditions in Argon and Nitrogen ($.01 < Km < 5$). The theoretical inviscid Mach Nos. ranged from 8.7 to 17.8 for nitrogen and from 15.0 to 25.6 for Argon. The data are compared

[†]See for example references 4 and 5.

with the available experimental results of other techniques as well as a suggested semi-empirical fit and theoretical models.

SECTION II
THE WIND TUNNEL BALANCE SYSTEM

A. The Magnetic Suspension System

Free electromagnetic suspensions controllable in one dimension have been in use since the 1930's. However, systems controllable in three dimensions having a wide applicability to problems of aerodynamic interest are relatively recent. In 1957 the concept of a three axis suspension system in which the forces on the supported object were automatically resolved into three independent, mutually-perpendicular components was devised by Parker.[6] Experimental verification of the concept was reported in 1959.[7,8] Development in a form suitable for use as wind tunnel balance was completed by 1964[9] and the present design became operable in 1965. This design as well as the general theory of operation has been described in the literature.[10,11,12]

The actual coil system used in the present apparatus does not follow any ideal configuration precisely, but rather utilizes a compromise arrangement conceived for the specific application. The major criterion was maximum force capability in the vertical direction while maintaining a reasonable tunnel size. The system provides independent three dimensional control and results in a linear relationship between applied force and coil current.

1. Coil Sets

The coil system is shown in Figure 2.1. A pair of large coils, A, is used to provide a magnetic moment per unit volume in the model. Gradient coil pairs, B. C, are located within the core of the main field coils and produce forces on the model in accordance with the general relation

$$\vec{dF} = (dm \cdot \nabla)\vec{B} \tag{2.1}$$

An analysis of these magnetic forces as a function of gradient coil geometry is given by Jenkins and Parker,[7] and there is a wide variety of

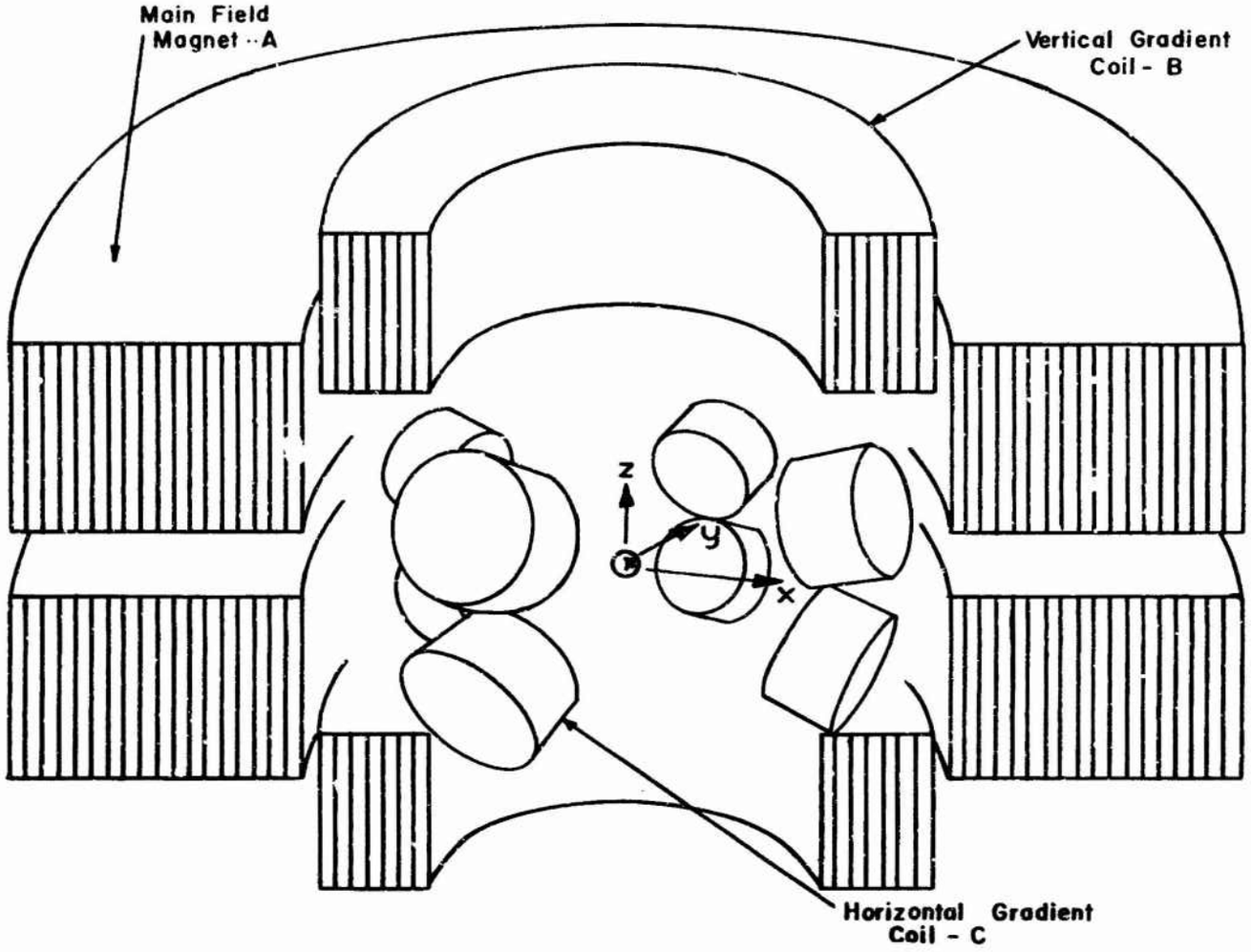

FIGURE 2.1 Coil Configuration

geometrical arrangements, including the one used here, which will produce forces readily resoluable into three mutually orthogonal components.

The airflow is directed vertically downward and hence the current on the vertical gradient coils is directly proportional to the drag on the model. In the case of the sphere, the gradient coil sets producing forces in the horizonal plane are used only to provide lateral stability.

2. Servo Control

The inherent instability of a magnetic suspension system requires a servo control system for each of the three degrees of freedom. The "error" signal to actuate this control is provided by two light beams at 90° in the horizontal plane. After passing over the model, each beam falls on a separate pair of photodiodes located symmetrically about the axis of the sensor system. Thus any motion of the sphere from its null position will generate changes in output of the photo diodes. When properly compared these outputs will yield appropriate signals in each of the orthogonal directions. With proper processing these signals are used to vary the currents in the respective gradient coil sets so as to maintain the sphere at the null position. A measure of the current change required is a measure of the force causing the displacement.

3. Force Calibration

A calibration was made to verify linearity and account for any gradient that might occur due to coil asymmetry. Initially the gradient coil pair symmetry plane was located as accurately as possible with a differential gaussmeter. Then one of the main field coils was shunted until the symmetry plane of these coils coincided with the zero field plane of the vertical gradient coils. This fixed the position of sphere support in the field.

For a calibration of force against gradient coil current nonmagnetic weight must be added to the spheres so that the magnetic moment induced by the main field at fixed field current remains constant as the load force is increased. In addition, any such dead weight must be added symmetrically

to avoid applied torque since the spheres have a preferred orientation in the field. Finally, the resulting diameter cannot be significantly larger than the original sphere and be compatible with the optical sensing system.

The techniques used to produce this calibration weight included the application of various coatings to the spheres and the attachment to the spheres of small brass rods in line with the magnetic moment.

A number of calibration runs were performed over the period that the data were taken. Both 1 mm and 1/8 inch diameter spheres were used and the results were repeatable. The last such calibration is shown in Figure 2.2. Each point represents a number of "weighings" with the same calibration sphere. Eleven different spheres were used and both operational modes of zero and 25 mv fixed gradient were checked. The data were fitted to a straight line with a standard deviation of 0.108 mv and a probable error of ± 0.0728 mv. The y intercept was - 0.65 and the sphere drag data includes this force correction. The probable error is ± 0.17% at the sphere weight (no load condition) and since all forces were measured as the sum of drag and weight (within the actual calibration range) the probable error in any total force measurement would be $\leq$ 0.17%. The repeatability with the "clean" spheres used for the drag measurements was ± 0.2% of sphere weight and the noise level was generally less than 0.2% under operating conditions. The calibration was checked by "weighing" each sphere under zero gas load before each run and after those runs during which the sphere was not lost. It should be noted that the calibration includes the least accurate force measurements made due to the difficulty of eliminating irregularities in the calibration models. Hence the balance is believed to be more accurate than is illustrated by the data.

The basic models were chrome steel alloy spheres and their masses and sizes are given in Table 1.

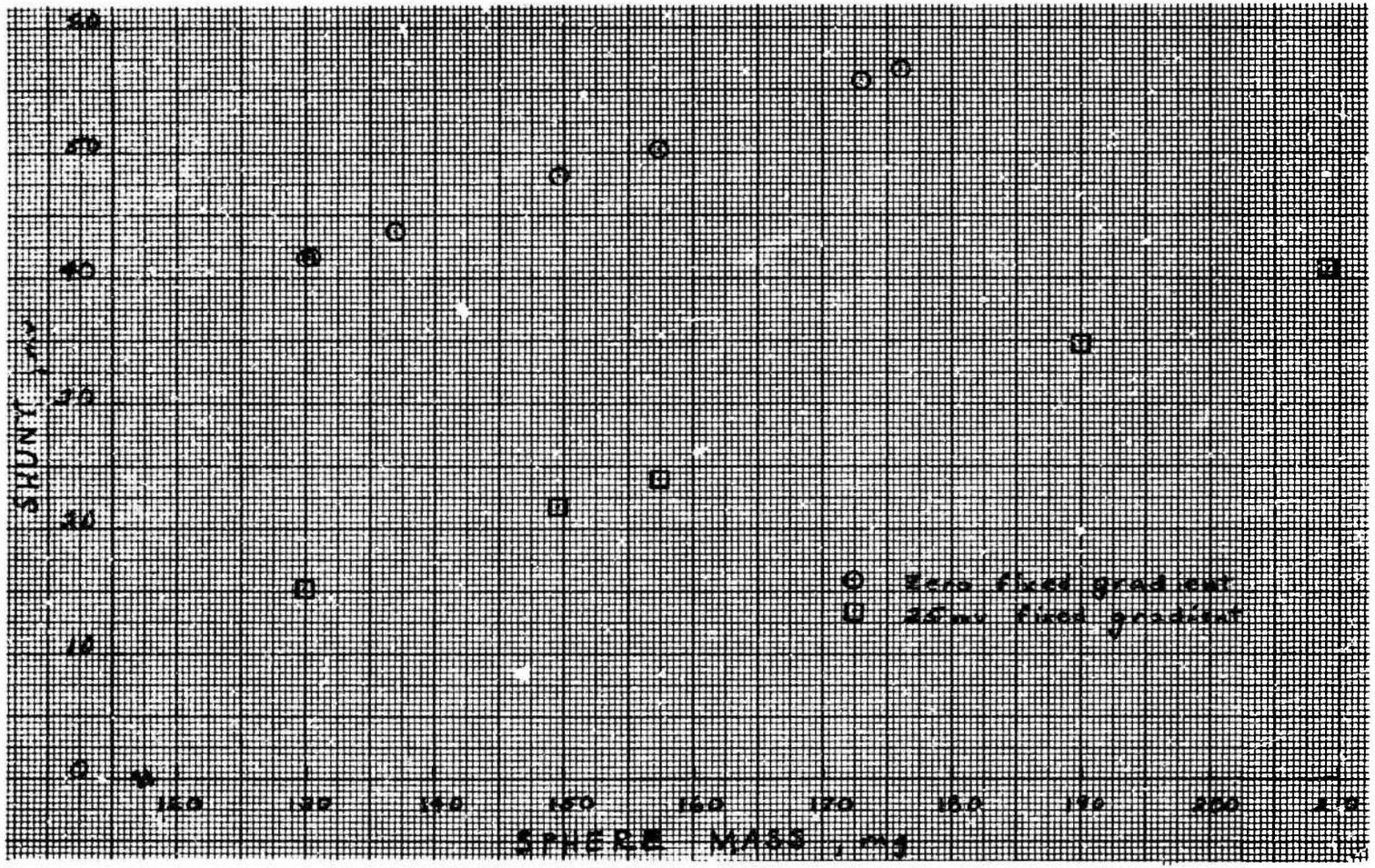

FIGURE 2.2 Balance Calibration

TABLE I

SPHERE MASS VALUES

Sphere Diameter	Mass (mg)
1/8 in.	130.0 ± 0.2
1 mm	4.8 ± 0.01
0.025 in.	1.045 ± 0.010

B. The Wind Tunnel

The free jet used as a flow field expands from a small converging nozzle into an eight-inch diameter vertical lucite cylinder. This section passes through the center of the magnet arrangement and contains optical windows for passing servo system light beams. The cylinder is evacuated by a Roots 615 booster pump in series with a Stokes 412 H Mechanical pump. Bellows were provided to reduce the transmission of vibration to the support system.

This system has a flow capability of about 1200 cfm of dry gas and the tunnel pressure was about 10^{-3} torr under no gas load. The characteristics of the system are such that the background pressures rises as the source pressure is increased. The ratio of source to background pressure remains nearly constant for a given nozzle under test conditions.

It is necessary to provide for alignment of the nozzle with the sphere and for the positioning of the nozzle relative to the sphere, since the flow properties in the jet are dependent upon the axial distance from the nozzle exit.

Also, a semi-automatic sphere-loader was devised so that models can be placed in support without opening the flow system. This is of considerable practical convenience.

C. Experimental Procedure

Selected spheres were cleaned and inserted into the loading chamber. The loading device was placed in the vacuum chamber and the system sealed. The system could be evacuated within a few minutes to about 10^{-3} torr. Lateral and vertical nozzle adjustments were made and the desired nozzle-sphere separation was established.

With the sphere in position the main current was increased to allow the sphere to rotate to its preferred orientation in the field. The gradient coil currents were activated and the vertical current was increased until the sphere lifted slightly from the loading device. The loader could then be lowered completely out of the test section region. Spheres would remain suspended in this mode under no gas load for long periods of time without noticeable drift or further adjustment. Recording the sphere support current (in the vertical gradient coil) under no gas load conditions provided a force calibration check for each test run.

Flow was established by admitting gas to the nozzle from a dry gas bottle through a two stage regulator and needle valve. A more sensitive nozzle alignment could then be performed by adjusting the nozzle position for zero lateral force on the sphere. Local properties could be varied by adjusting the nozzle-sphere separation or by varying the source pressure.

A data run consisted of incrementally increasing the source pressure and recording the support current at each increment with the nozzle-sphere separation remaining fixed.

Ideally, the source pressure was increased until the maximum force capability of the balance was approached and then decreased to zero to provide a final check on the force calibration. (In practice, however, the sphere was often lost during the run.) The model position in the field was carefully maintained by adjustments during the run.

Gas could be admitted directly into the vacuum chamber to vary the pressure level at constant source conditions. The sensitivity of the force measurement to the chamber pressure level or the pressure ratio was checked for each set of nozzle conditions.

SECTION III

THE FREE JET FLOW FIELD

A. Jet Geometry

The characteristic dimensions of the free jet have been determined by Bier and Schmidt[4] using Schlieren photographs and by various authors[†] using other techniques and with a number of gases. These dimensions are a function of the nozzle size and the ratio of source pressure to background pressure, P_c, outside the jet. The core flow is contained within oblique shocks and the nearly normal shock or Mach disc downstream. When the proper ratio of stagnation to background pressures, P_o/P_c, is maintained and the background pressure is sufficient for the shocks to be well formed, the core flow is independent of the chamber pressure and may be described by isentropic assumptions.

The most important dimension when using the jet as a flow field is the axial distance to the Mach disc. This may be expressed as[5]

$$\frac{x}{d_n} = 0.67 \left(\frac{P_o}{P_c}\right)^{1/2}$$

independent of the gas used for $15 \leq P_o/P_c \leq 17{,}000$. The absolute dimensions of the jet flow field are relatively fixed for a given pumping plant. For the wind tunnel balance system the Mach disc was about 32 mm or more downstream for both nitrogen and argon.

B. Flow Variables

Since the flow properties in the core flow vary along the jet axis, the local conditions at the model can be altered by adjusting the nozzle-sphere separation as well as the source pressure. Variables characterizing the flow field can be calculated using familiar gas dynamic concepts. A Knudsen number defined as

[†]See bibliography.

$$Kn = \frac{\lambda}{d_s} \tag{3.2}$$

is easily obtained if it is assumed that $\rho\lambda$ = Constant on the jet axis. This implies that the gas collision cross-section can be evaluated at stagnation temperature. The assumption may not be unrealistic since the sphere is approximately at stagnation temperature. (This is discussed in Chapter V). The Reynolds number behind a normal shock,

$$Re_2 = \frac{\rho_2 V_2 d_s}{\mu_2} \tag{3.3}$$

can also be evaluated.

Familiar nondimensional variables based on local free stream conditions require a knowledge of the local temperature and viscosity. Due to the nonequilibrium nature of the flow at the large distances downstream encountered here, different temperatures may be obtained perpendicular and parallel to the jet axis.† This is further complicated by the "freezing" of the parallel temperature at certain values of $P_o d_n$ while the perpendicular temperature continues to decrease in a manner similar to the isentropic prediction. Even if the manner of combining these values were clear, viscosity data at the resulting low temperatures is open to question. However, certain comparisons require a free stream Knudsen number and for these purposes an expression based on the Lennard-Jones potential model will be used. The resulting Knudsen number is

$$Kn_\infty = \frac{1}{\sqrt{2}\, n_\infty \pi \sigma_d^{\,2} \Omega d_s} \tag{3.4}$$

where Ω is tabulated in Hirschfelder, Curtis and Bird[16] and σ_d is the hard sphere molecular diameter. The value Ω is obtained by extrapolation and based on the isentropic temperature value for convenience. It should

†See for example Muntz[15].

be noted that in addition to the fact that such a calculation is at best very approximate, it is not at all clear that this is a reasonable parameter for correlating drag data. In any event, calculation of Ω based on typical freezing values of T_{11} do not significantly alter the results used here.

C. Effective Nozzle Size

Nozzle throat viscous effects are important at low densities as has been indicated by Ashkenas and Sherman,[5] Reis,[17] Lefkowitz,[18] and others. The jet flow should scale as some effective nozzle diameter which is a function of the nozzle (or orifice) shape as well as the throat Reynolds number. Although it is not certain that the correct effective size is that determined from mass flow discharge coefficients, it appears that the use of such a diameter would be more realistic than using the actual throat size at the low throat-Reynolds Nos. encountered in the sphere drag experiments.

Thus mass flow measurements, taken with three nozzles (each having a different profile were used to calculate the effective nozzle diameter as a function of Reynolds number assuming sonic conditions at the throat. The effective diameters, normalized to the actual throat diameter, are shown in Figures 3.1 and 3.2 for nitrogen and Figure 3.3 for argon. Variations in geometry bring about different results for each nozzle. The 1.1 mm diameter nozzle had a smoothly varying profile approximately exponential in shape. The 2.1 mm nozzle was conical, fairing into a straight section at the throat and the 0.95 mm nozzle was a relatively thick orifice.

This effective nozzle size was used to calculate the jet flow properties. It is interesting to note that the 1.1 mm nozzle results and the orifice results are in agreement with the values obtained by Ashkenas[5] using impact pressure measurements (there is a slight discrepancy in the high Reynolds number asymtotes indicated). Lefkowitz[18] also found agreement in effective nozzle size implied by impact pressure measurements and mass flow values.

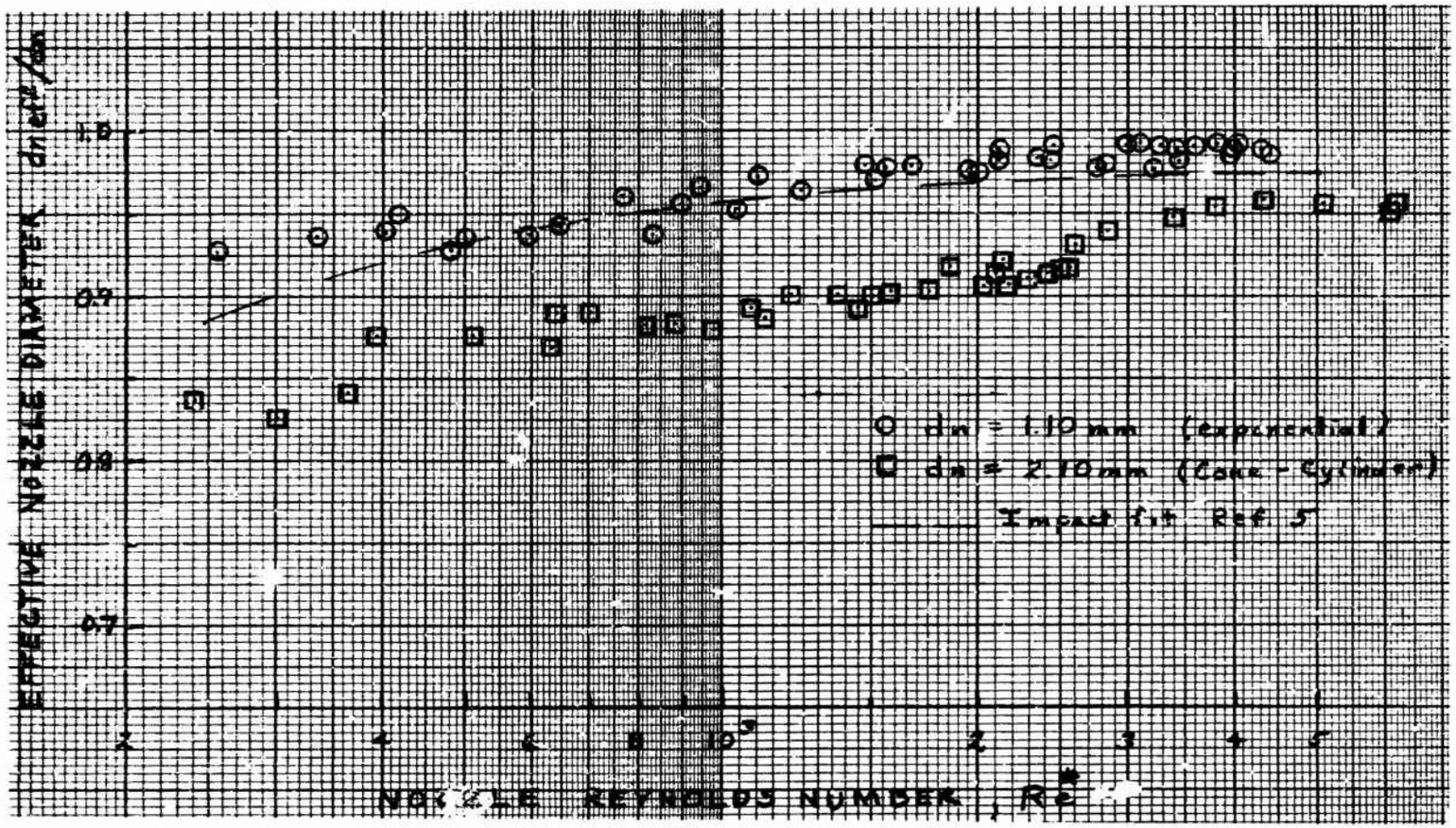

FIGURE 3.1 Mass Flow Measurements with Nitrogen (shaped nozzle)

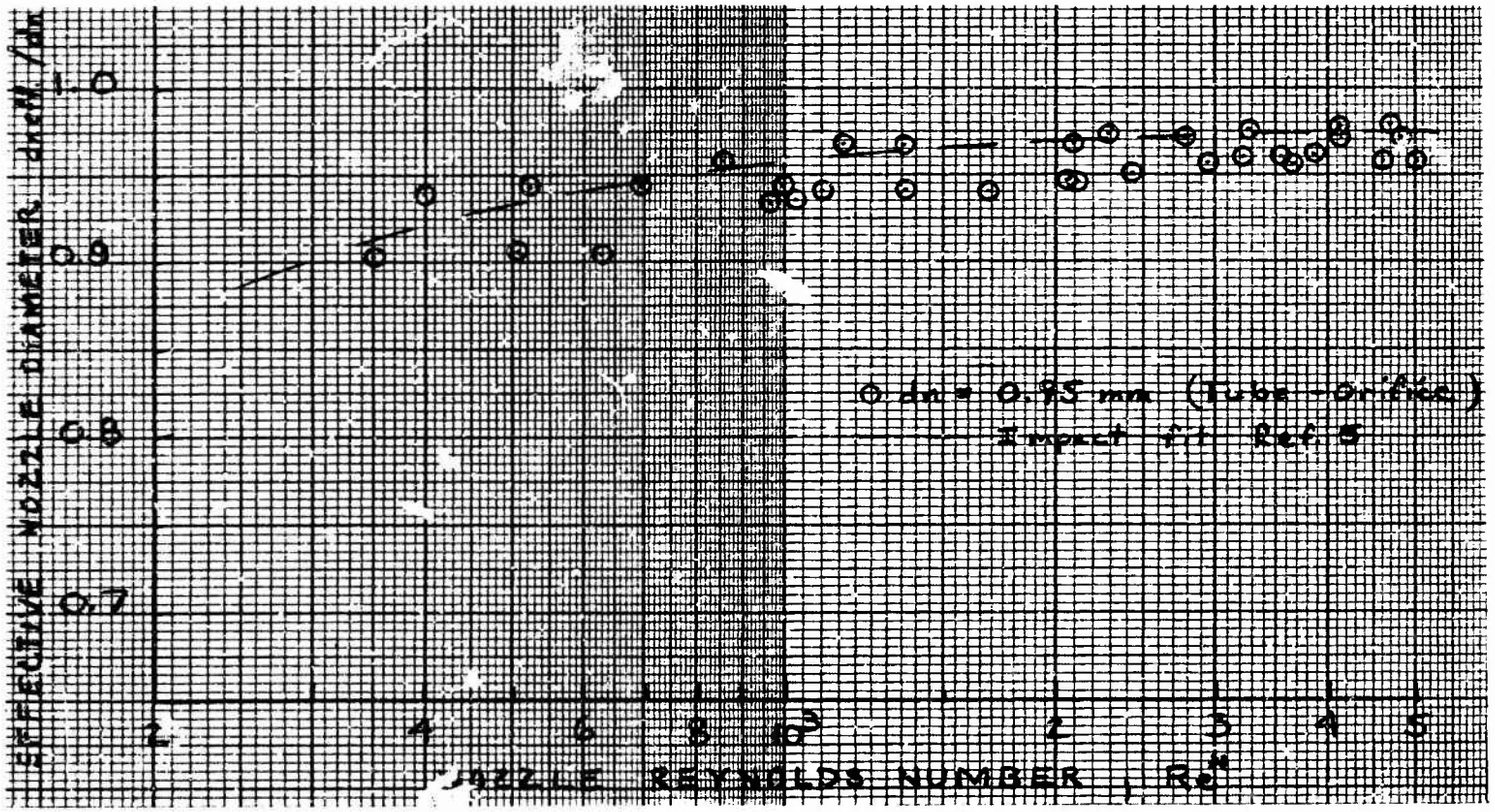

FIGURE 3.2 Mass Flow Measurements with Nitrogen (tube; orifice)

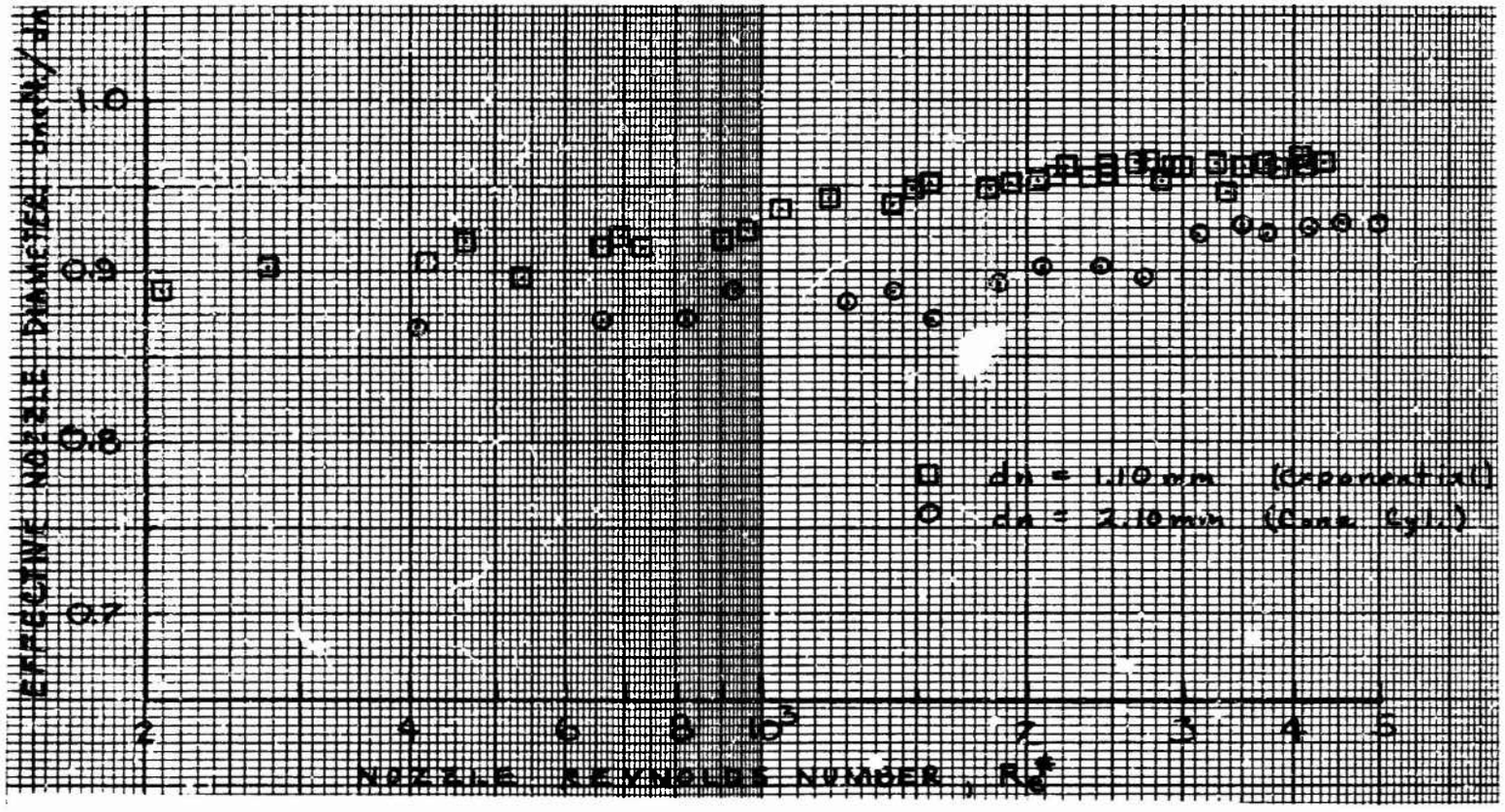

FIGURE 3.3 Mass Flow Measurements with Argon (shaped nozzle)

D. Flow Gradients

The gradients resulting from the expanding nature of the flow must be considered if a correlation is to be made with results obtained in a uniform stream. The effect of these gradients for drag purposes can be characterized by the variation in density since the velocity is essentially constant at large nozzle-sphere separations.

Ashkenas[5] gives an expression for the radial variation of density that predicts the characteristics calculation within about 3%. This equation is

$$\frac{\rho(r,x)}{\rho(0,x)} = \cos^2\theta\cos^2\left(\frac{\pi\theta}{2\phi}\right) \tag{3.5}$$

where r is the radial distance perpendicular to the jet axis and

$$\theta = \tan^{-1}\frac{r}{x - x_o} . \tag{3.6}$$

The constant ϕ has the value of 1.662 for nitrogen and 1.365 for argon and $\frac{x_o}{d_n}$ is 0.40 and 0.075 respectively. A calculation for the worse case encountered in these measurements (largest sphere, smallest s/d_n, argon) shows that

$$\frac{\rho(r,x)}{\rho(o,x)} \sim 0.96 \tag{3.7}$$

at the maximum r. This, however, overestimates the effect since the flow nearer the stagnation streamline is more effective in transferring momentum to the sphere. On the basis of this premise and the fact that most of the data is taken farther downstream and/or with smaller spheres, the radial variation in flow properties is neglected. Radial impact surveys by Ashkenas[5] also indicated a negligible variation of Mach number or impact pressure over a few nozzle diameters about the axis for large nozzle-probe separations.

The effect of axial gradients on the drag is somewhat more difficult to assess. One criterion is that $\frac{\partial \rho}{\partial x} / \rho$ be negligible over d_s. This may be too stringent a requirement since in hypersonic low density flow only the front half of the sphere is effective. In any event, the neglect of axial gradients when using the larger spheres may be questioned. The situation may be further complicated when considering nearly free molecular flow. Since the molecules reflected from the front of the sphere "see" an increasing density gradient upstream, perhaps more of them are scattered back onto the surface than would be the case in a uniform stream. On the other hand, radial gradients would tend to remove more molecules from the area. The results reported here are based either on the density of the sphere center location or the stagnation point and axial gradients are not otherwise accounted for.

E. Effects of Temperature and Background Gas

The effect of "freezing" of the temperature and Mach number at the lower values of $P_o d_n$ on the experimental drag coefficient is negligible and hypersonic conditions are maintained. There are some problems due to the appearance of the free stream temperature and speed ratio in the theoretical expressions and these effects are considered when they occur.

A most important consideration in using the free jet as a flow field is the effect of the background gas and shock system on the core flow. These effects have been investigated by a number of authors[†] with particular emphasis on criteria for maintaining an isolated core flow. It has been maintained that the Mach disc location can be calculated, however the extent of its influence upstream of this "position" due to thickening at low background pressures is not so clear.[‡] The oblique side shocks must also broaden as the density is lowered and may, at some

---

[†] See for example References 4, 19, 20, and 21.

[‡] Bier and Hagena[19] indicated that the Mach disc became diffuse enough to disappear from flow photographs as a Knudsen number defined as $\hat{Kn} = \lambda_c / Y_m$ approached unity.

point, influence the centerline properties. At low enough background pressures the jet may become "porous" to background gas and the core flow can be influenced by the chamber pressure. Although the results of these effects and the values of parameters characterizing them are perhaps not satisfactorily determined in general; it is clear that these effects are to some degree a function of P_o/P_c and/or the absolute value of the background pressure. Since the core flow must be independent of the chamber pressure for the assumptions and calculations used to be valid, the drag force must not be influenced by a reasonable variation in background pressure. The chamber pressure was varied in the tests reported here and data affected by such a variation will be noted and considered to be in error.

Finally the possibility of condensation can be considered. Molecular beam experiments indicate that no condensation occurs at the conditions encountered for nitrogen. For argon some condensation may be present but no effect on the data was observed.

SECTION IV
EXPERIMENTAL RESULTS

A. General Discussion

Drag data taken at axial positions from 10 to 22 nozzle diameters downstream† are normalized in the form of a drag coefficient and presented as a function of a number of familiar flow variables. The selection of the independent parameters was influenced by comparisons with available experimental and theoretical results as well as an attempt to determine a representative variable for drag in transition flow that could be calculated with reasonable accuracy. Variation of the nozzle size and the axial position of the sphere allowed an increased range of transition flow to be investigated and provided assurance that the results were not specifically related to the nozzle or jet geometry. Three sphere sizes were used to cover a wider range of the independent variable. The flow properties are calculated at the location of the center line except where otherwise notes.

The results are divided roughly into three groups corresponding to small ($\frac{x_s}{d_n}$ ~ 10-13), intermediate ($\frac{x_s}{d_n}$ ~ 13-18) and large ($\frac{x_s}{d_n} \geq 22$) nozzle-sphere separations. However, this division is not rigorously maintained and some overlap will be obvious in the presentation. The selection is arbitrarily made to show the agreement of the data taken at these stations. A difference was evident when comparing the data taken close to the nozzle and that taken at the largest distances downstream. At fixed Knudsen number, the drag coefficient data is systematically higher for stations close to the nozzle, and decreases with increasing x_s/d_n. This trend is reduced by calculating the flow properties at the position of the sphere stagnation point on the jet axis instead of the center location. The results of this analysis are given in sections V and VI.

---

†One additional station was taken at 54 nozzle diameters with the 0.445 mm nozzle.

B. Drag Measurements with Source and Model Initially at Room Temperature

The drag coefficient for nitrogen is presented as a function of the Knudsen number (assuming $\rho\lambda$-const.) for low to high values of nozzle-sphere separation in Figures 4.1 through 4.3. Figures 4.4 and 4.5 present similar results for argon. For all data the source temperature was about 298°K. Theoretical inviscid Mach numbers ranged from 8.7 to 17.8 for nitrogen and from 15.0 to 25.6 for argon.

Data outside of the vertical lines shown on the figures are noted to be in error and the effect of the background pressure variation on these data is given. Although these limits could often be determined by examining the graphs, they were obtained experimentally in each case by recording any change in force with independent variation of the chamber pressure at constant source conditions. The position of the vertical line excludes the values of Knudsen number at which the smallest recordable change in force (< 0.3% of sphere weight) occurred with a reasonable increase in background pressure (obviously an unlimited increase in P_c always produced an effect). Although such a determination is admittedly qualitative, the agreement with the inflections observed in the drag curves indicates that the test is valid. The limits were recorded for each sphere size and occurred at approximately the same source pressure for a given nozzle-sphere separation. Clearly these limits appear at different Knudsen numbers as a function of sphere size but only those for maximum Knudsen number with the 0.635 mm sphere and minimum Knudsen number with 1/8 inch spheres are shown. All intermediate points affected are omitted for clarity since a valid point could be obtained at that Kn under another set of conditions. One adidtional verification of the "unaffected" data is provided by the fact that the curves for different sphere sizes are in agreement and in many cases an area of overlap is shown. The data influenced by the background pressure variation do not agree in this manner.

The exact nature of the influence of jet shock structure and background pressure on the core flow has not been quantitatively resolved. Measurements of sphere drag, however, do not represent a satisfactory

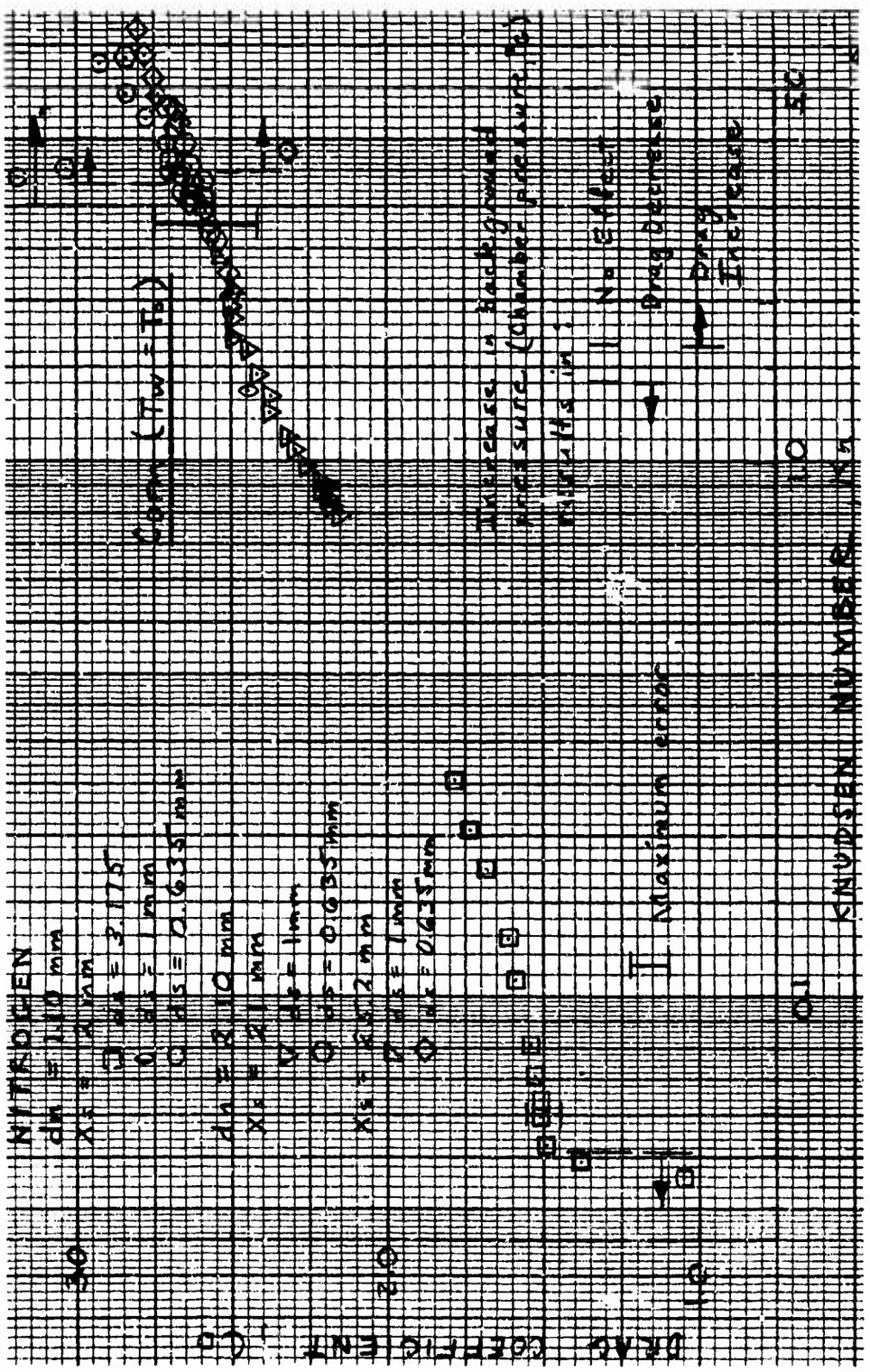

FIGURE 4.1 Sphere Drag vs. Knudsen No. (Low x_s/d_n) for Nitrogen

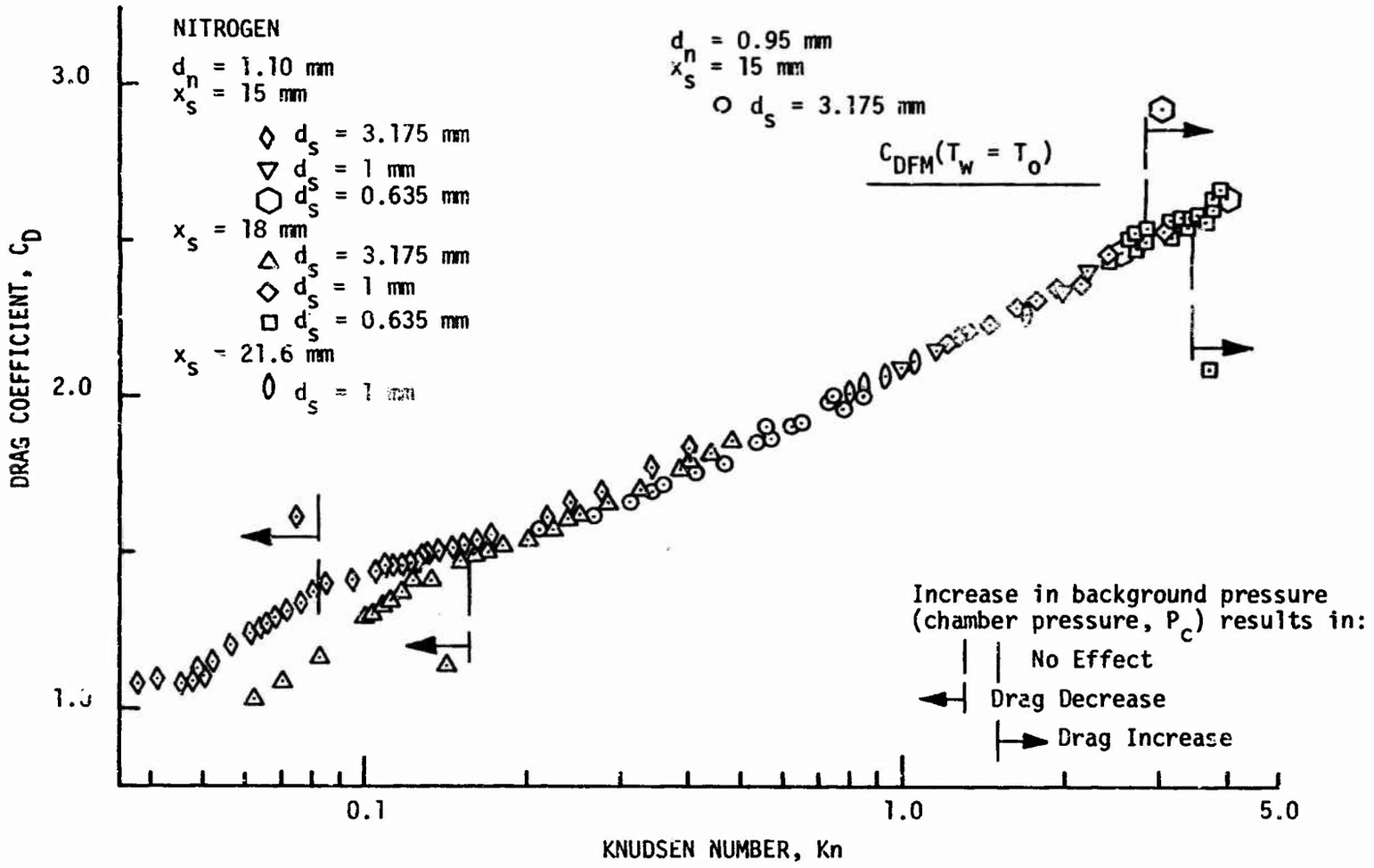

FIGURE 4.2 Sphere Drag vs. Knudsen No. (Int. x_s/d_n) for Nitrogen

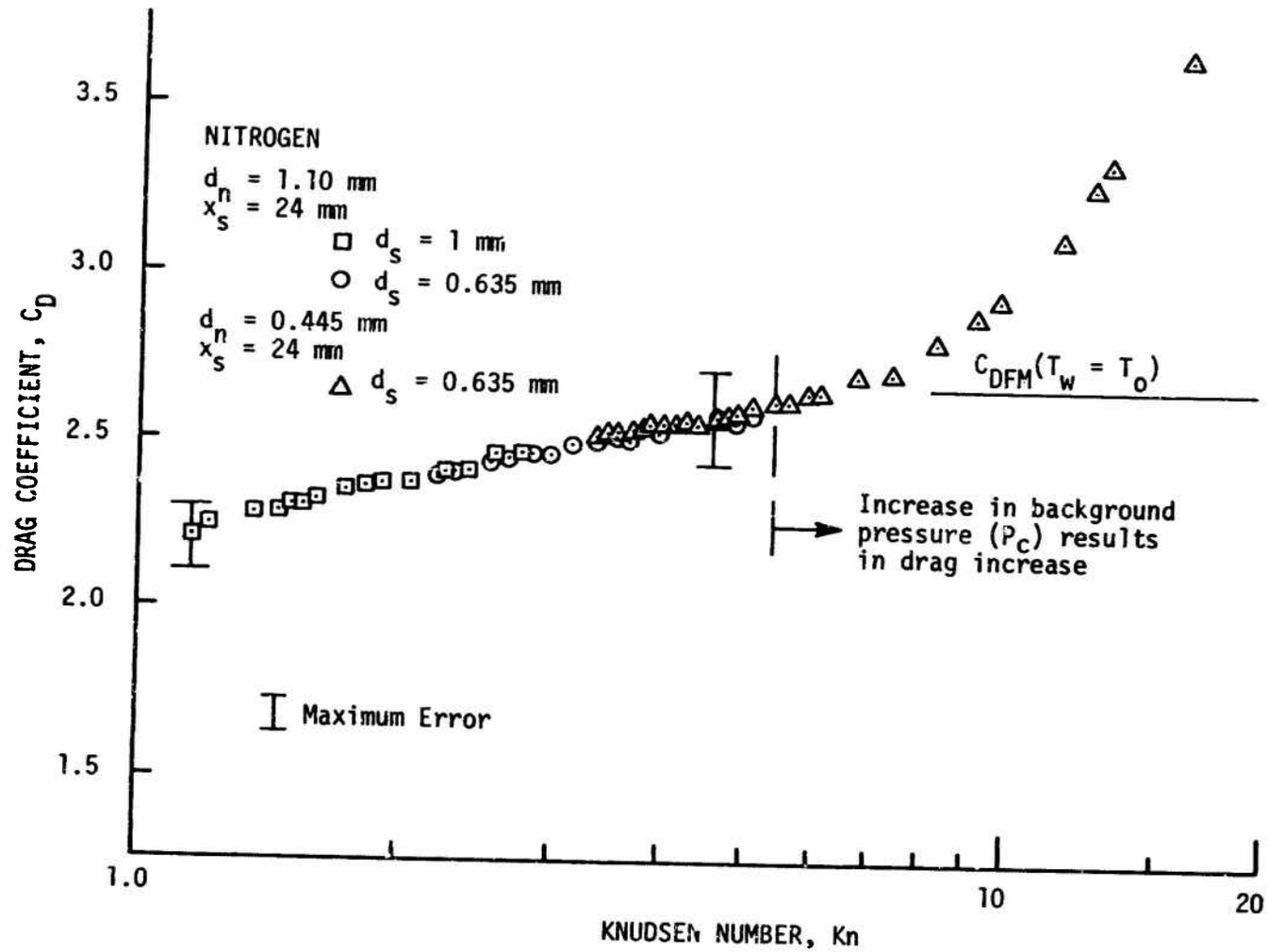

FIGURE 4.3 Sphere Drag vs. Knudsen No. (High x_s/d_n) for Nitrogen

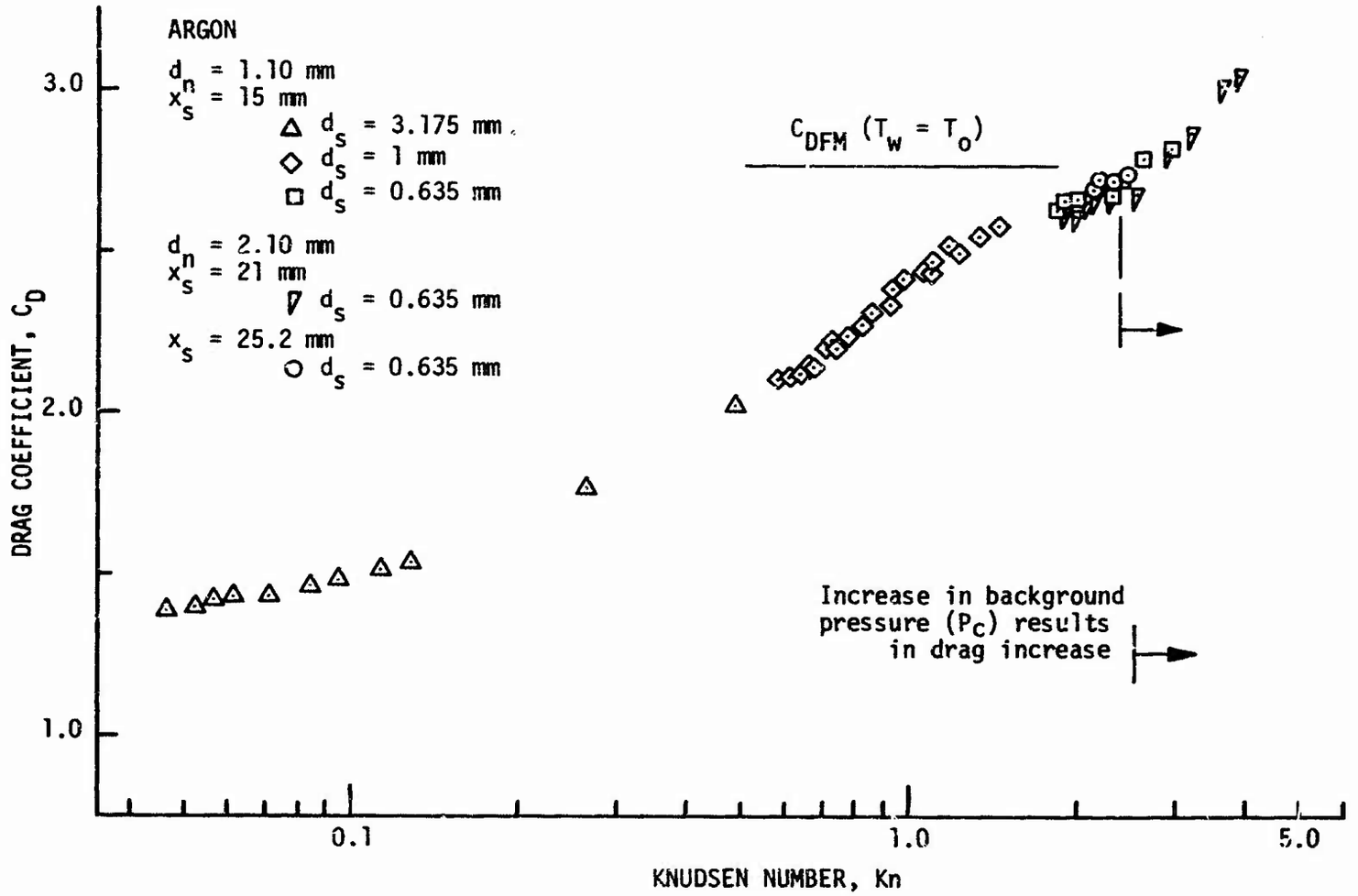

FIGURE 4.4 Sphere Drag vs. Knudsen No. (Low x_s/d_n) for Argon

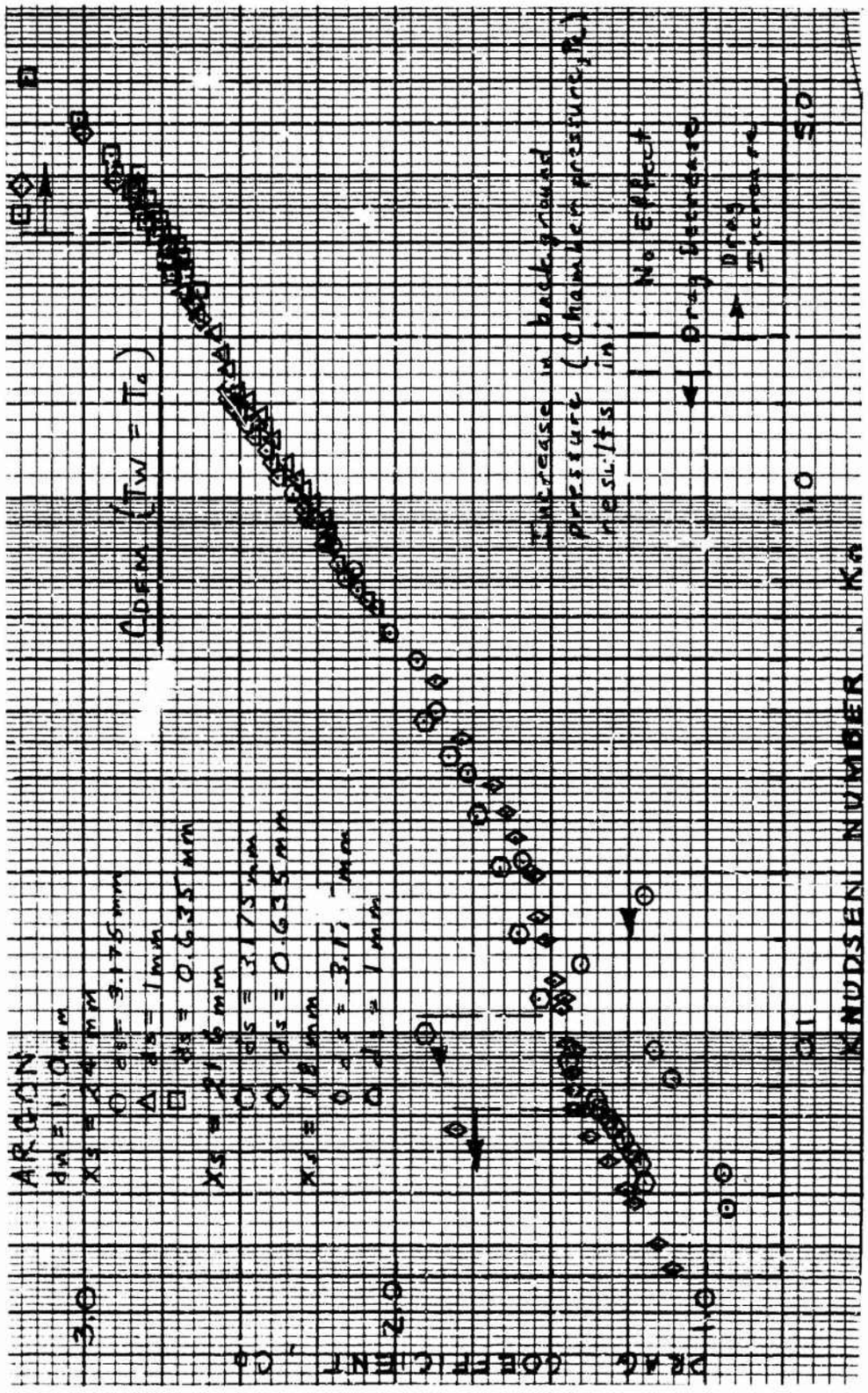

FIGURE 4.5 Sphere Drag vs. Knudsen No. (High x_s/d_n) for Argon

method for determining the details of these effects. The sensitivity of the balance does provide an accurate indication of the onset of such effects on the drag measurements and the fact that no sting extended through the shock structure assured that the effect was not precipitated by the influence of a mechanical support.

At high densities the sphere bow shock may be well formed. This shock, however, becomes a broadened density disturbance as the density is reduced. The jet Mach disc and oblique side shocks also broaden as the pressure is lowered.† Interactions between these shock structures, the sphere wake, and background gas appear to account for the effects observed. When the Knudsen number is high, the influence of background pressure causes an increase in drag. It is difficult to see how this can be attributed to the broadening Mach disc since one would expect a decrease in impact pressure as the tail of the shock is entered.‡ Perhaps an infiltration of gas through the side shocks and accelerated by the outer part of the jet increases the centerline impact pressure at low densities. Another possibility would be the influence of the continually broadening oblique side shocks contributing to this increase. These effects could not be distinguished by the techniques of this experiment.

The influence of background pressure on the measurements at high source pressures was a decrease in drag. Gregorek and Luce[20] have shown that the pressure on the downstream side of the sphere can be increased with little effect on the upstream face as the data is taken further downstream (closer to the Mach disc). The effect occurs even though the nominal position of the Mach disc is a number of nozzle diameters downstream of

†See references 5, 19, 20.

‡In fact this effect was observed during the tests. For a number of runs the measurements are taken at continually reduced source pressure and correspondingly reduced background pressure due to the characteristics of the system. The drag coefficient increased smoothly to a maximum and then decreased. Credit for the decrease is given to entering the Mach disc shock structure.

the sphere position. This appears to be borne out by the decrease in drag observed at low Knudsen numbers here. The decrease occurs later (at both lower Knudsen numbers and higher source pressures) if the sphere is positioned further upstream. Grek[20] shows that the sphere bow shock can actually be deflected by the jet shock structure.

It is not implied that the detailed nature of the interaction mechanisms are proved by the results presented here, but only that these effects could account for the results observed. More detailed analysis and careful experiments would be necessary in an attempt to make use of the data influenced by the jet structure and no such effort has yet been made. The data affected is noted to be in error and shown both to indicate that care was taken to assure the validity of the results presented and that such an investigation is essential when using the free jet as a flow field.

The free molecular limits shown in Figures 4.1 - 4.5 are calculated from[22]

$$C_{DFM} = \frac{2 - \sigma' + \sigma}{S^3}\left[\frac{4S^4 + 4S^2 - 1}{4S}\,\mathrm{erfs} + \frac{e^{-S^2}}{\sqrt{\pi}}\,(S^2 + \tfrac{1}{2})\right] + \frac{2\sqrt{\pi\sigma'}}{3S}\sqrt{\frac{T_w}{T_\infty}} \qquad (4.1)$$

with

$\sigma = \sigma' = 1$ diffuse reflection

$\sigma = \sigma' = 0$ specular reflection .

Since the stagnation temperature, the original sphere temperature, and the surrounding room temperature were the same for these tests, the sphere is assumed to be at stagnation temperature for the calculation.†

† An exception will be noted as T_w insulated.

The data generally indicate that this assumption is valid. The diffuse reflection limit was assumed since all of the data rise above the specular limit and indicate that the diffuse value is approached. Molecular beam experiments with a target of the same material as the sphere models also indicates diffuse reflection at room temperature.[†] Although the theoretical values of the speed ratio and free stream temperature used may be in error due to freezing at large nozzle-sphere separations and low source pressures, calculations based on roughly estimated frozen values[14,23] indicated that the effect was negligible for the calculation of C_{DFM}.

The most attractive feature of Kn as a flow parameter for correlating the data is that it can be accurately calculated. Values for viscosity (and hence mean free path) are not available at the local free stream temperatures encountered. However, since the molecules reflected from the sphere surface have energies corresponding to stagnation temperature, it appears that the effect of molecular collisons causing a departure from free molecular conditions might be better characterized by a Knudsen number based on source conditions than a parameter dependent on free stream properties. The data are presented as a function of other parameters elsewhere in this chapter.

A small amount of scatter in the results shown in Figures 4.1 - 4.5 is evident. The data includes all points for each run except where points are obscured by the density of the plot. No averaging or selection was employed to reduce the scatter. The apparent scatter is largely due to the presentation of data at different nozzle-sphere separations on the same plot. The runs were repeated and reproducibility was better than the scatter shown on the graphs.[‡] No effort was made to label separate runs at the same conditions, and often only one run is shown.

[†]Taken by the Gas-Surface Studies Laboratory, Department of Aerospace Engineering and Engineering Physics, University of Virginia.

[‡]The one exception is the data at 12 mm where some repeatability problems were encountered due to nozzle vibration. However, the run is representative and the difference was at worst ~ 5% with runs taken over the span of a year.

C. Drag Measurements with Source and Model Heated

A limited amount of data was taken with a heated source using the 0.95 mm nozzle and the results are shown in Figure 4.6. The purpose of source heating was to increase the local temperatures so that free stream properties could be calculated and with more confidence to move the Mach disc downstream. However, no significant gain was achieved at the source temperatures attained.

Due to experimental problems only the 1/8 inch spheres were used. The sphere temperature is now known and the nozzle position may have changed with increasing temperature. Some decrease in the drag coefficient might be expected if the sphere was cooled by radiation to the ambient surroundings but no such decrease was observed. Radiation from the heated nozzle may have compensated somewhat for this cooling. If the sphere was near the nozzle stagnation temperature, no effect of source heating on the drag coefficient would be expected unless the surface accommodation model changed. The parameter Kn may not be valid for correlating this data if the surface is cooled, however, the results remain slightly higher than the ambient data in terms of Kn_∞ or Re_2. Finally, the sphere magnetic moment and hence the calibration could be affected. It was concluded that no measurable change in drag coefficient due to source heating could be determined from these results.

One positive result is indicated by the curve. The maximum rise in the data due to jet influence is reduced by heating the source. This might be expected since the flow field size increases as $(T_o)^{1/4}$, indicating that heating the source should provide an increased data range. However, better control over the heating process, considerably higher temperatures, and careful calibration would be essential for any significant improvement.

Attempts were made to heat the sphere surface and monitor the surface temperature using infrared techniques. The results are shown in Figure 4.7. Again the variable Kn may not be the correct correlating parameter for these data if the scattering is diffuse. However, qualitatively the

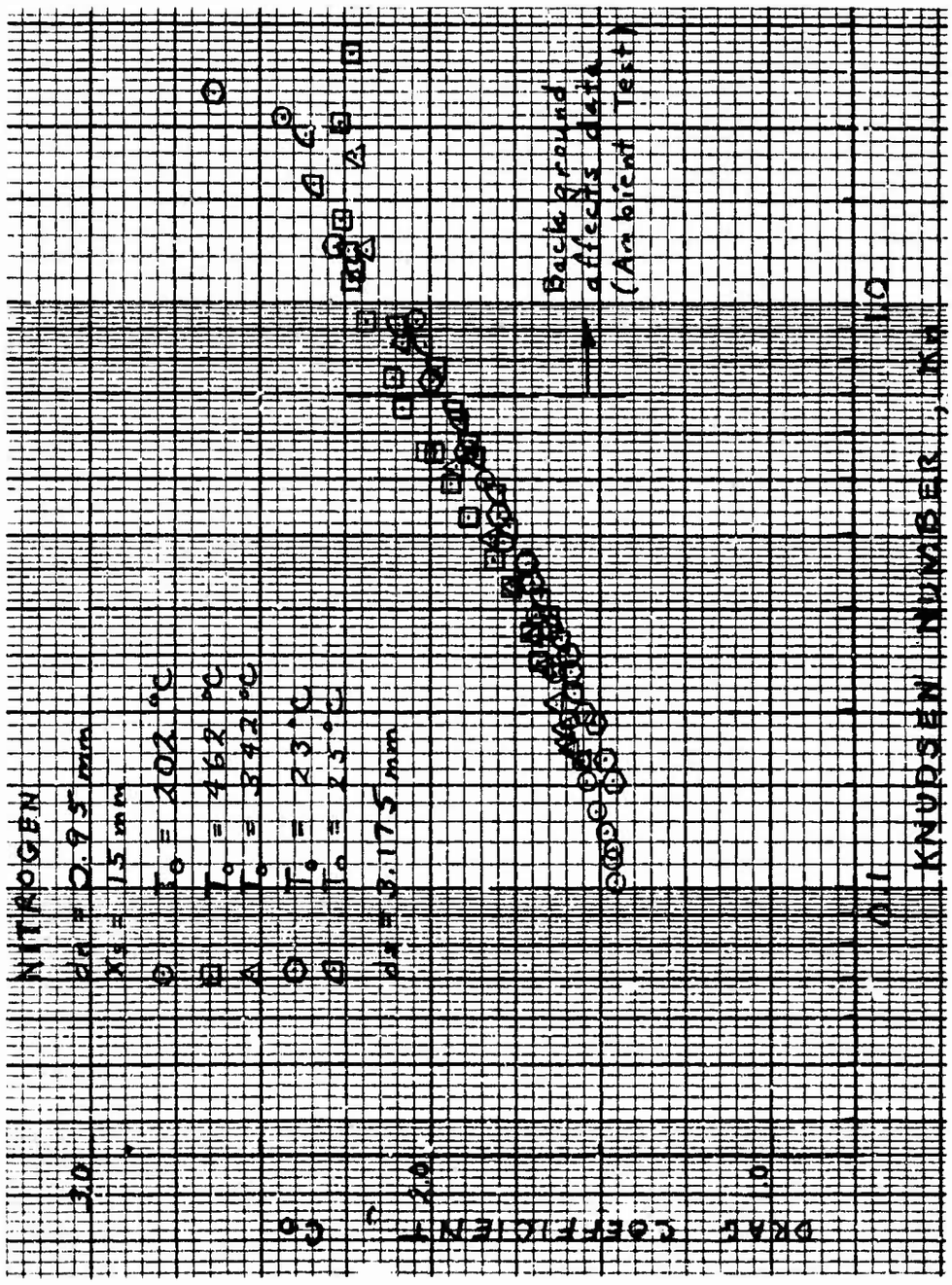

FIGURE 4.6 Source Temperature Effect on Sphere Drag

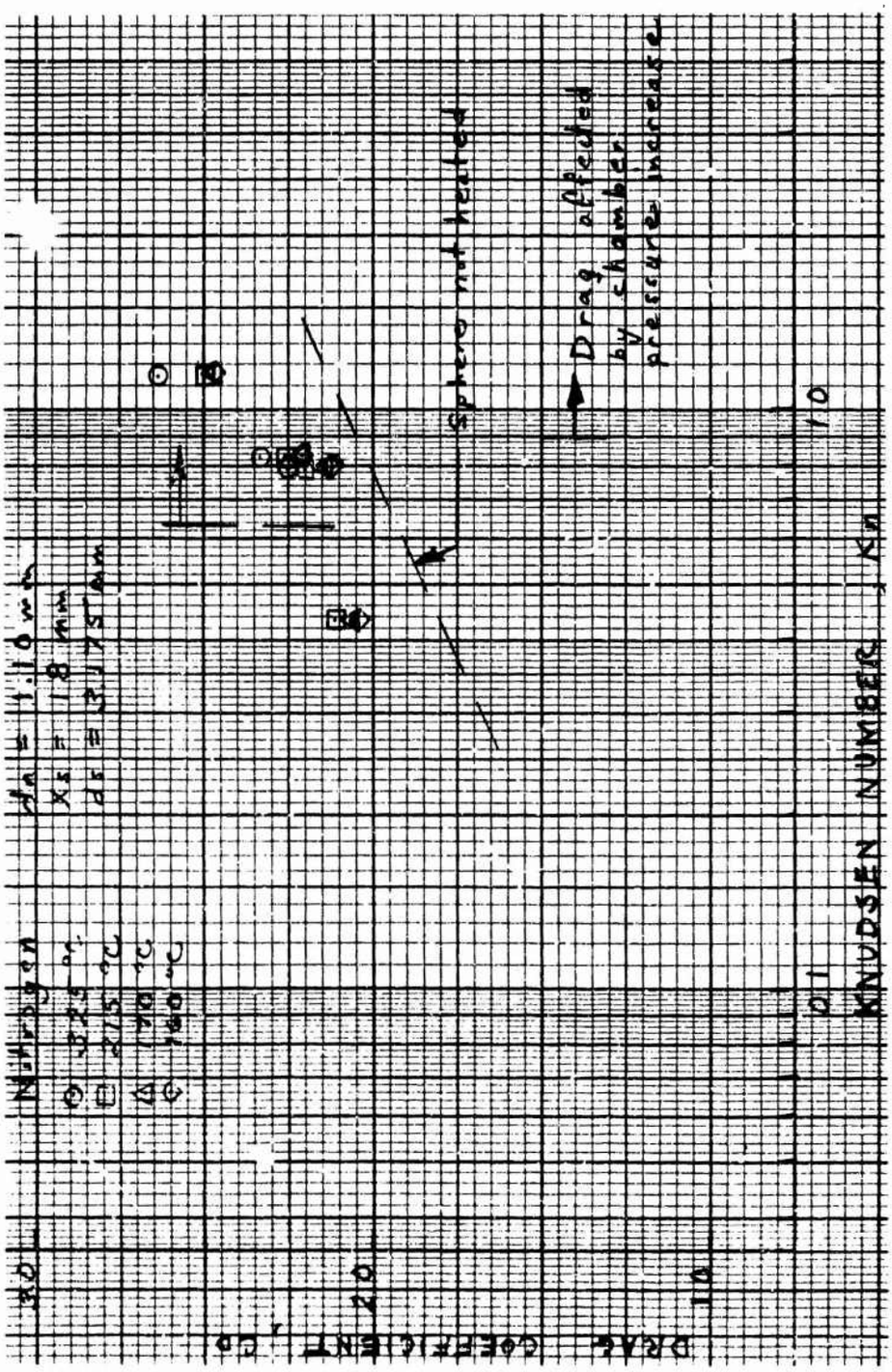

FIGURE 4.7 Drag Coefficient for Heated Spheres

increase observed indicates diffuse reflection since no change would be expected if the scattering were specular. These data would be more valuable near free molecular flow but such results were not successfully obtained. Calculation of the increase in drag expected in free molecular flow for completely diffuse reflection indicates that, at least when correlated in terms of Kn, the measured increase in C_D due to surface heating is approximately the same or greater than the calculated increase (ΔC_D ~ 0.2 @ 215°C). This measured difference would be less if some increased effective Knudsen number were used that included the effect of the increased body temperature.

D. Discussion of Experimental Error

An estimate of the error in the measured quantities is as follows:

P_c	(0-20 torr)	± 0.05 torr
P_o	(>20 torr)	± 0.5 torr
d_n	(1.10 mm)	± 0.01 mm
	(0.95 mm)	± 0.04 mm
	(0.445 mm)	± 0.005 mm
T_o		± 0.5°C
d_s	(0.635 mm)	± 0.0013 mm
	(1 mm)	± 0.0013 mm
	(3.175 mm)	± 0.0025 mm
nozzle position		± 0.05 mm
sphere mass	(0.635 mm)	± 1%
	(1 mm)	± 0.25%
	(3.175 mm)	± 0.15%
force (reading error)		~ ± 0.25% of sphere support current
force (calibration)		< ± 0.2%
d_n effective (from mass flow)	scatter	~ ± 1%
	calibration	± 0.5%

The error resulting from the use of the theoretical equations[5] is:

P_i/P_o ± 1%

M ± 1/2%

If the above errors are all added, the maximum possible error is ~ 4.5-6.8% (from low to high Knudsen numbers) in the drag coefficient at the smallest nozzle sphere separation. The error is less for larger distances downstream. Typical maximum error flags are shown in Figure 4.1 and 4.3. Repeatability of the data is much better than these maximum possible error values.

The error due to axial and radial gradients in the flow field has been discussed. The radial gradients are considered negligible and the axial gradient problem is believed to be a minimum when the flow properties are calculated at the sphere stagnation point location. The error due to gradients is considerably less for large nozzle-sphere separations, indicating a preference for these data.

SECTION V
COMPARISON WITH RESULTS OF OTHER EXPERIMENTS

A. Flow Properties Based on Sphere Center Line

The current literature on the measurement of sphere drag at low densities contains data obtained by a number of different techniques and representing a wide range of key variables such as the Mach No. and Knudsen No. In order to make a meaningful comparison of these data some correlation parameter must be used. Although the literature also contains much discussion concerning the proper choice of correlation parameter, one that seems to have received relatively wide-spread use is the Reynolds No. downstream from a normal shock as computed by isentropic theory. We have arbitrarily chosen this as the independent variable or correlation parameter and have denoted it as Re_2.

In Figure 5.1 the results of the previous section are presented as a function of Re_2, where the dependent variable is the drag coefficient normalized to the free molecular diffuse value with the sphere at stagnation temperature. This presentation is also consistent with that of many other authors. Also shown on this figure are the free flight data of Kinslow and Potter[24] for nitrogen, Bailey[25] for air and the free flight shock-tunnel results of Geiger[26] for air. All of the results of Kinslow and Potter are presented. Bailey's data continues to much higher Reynolds numbers than are within the range of the graph. The reduction in scatter with the magnetic suspension technique is evident and can be even less if data at only one sphere station is presented. An extension of the data toward free molecular flow is provided by the present technique and although it appears that the free molecule limit is attained, the data to the left of the vertical line are of questionable validity due to the influence of the jet structure. This again points out the need for caution when using the jet flow field.

All of the free flight results are for relatively cold wall conditions. This suggests that the present results should perhaps be greater than the free flight data. This increase is not apparent in the comparison. However,

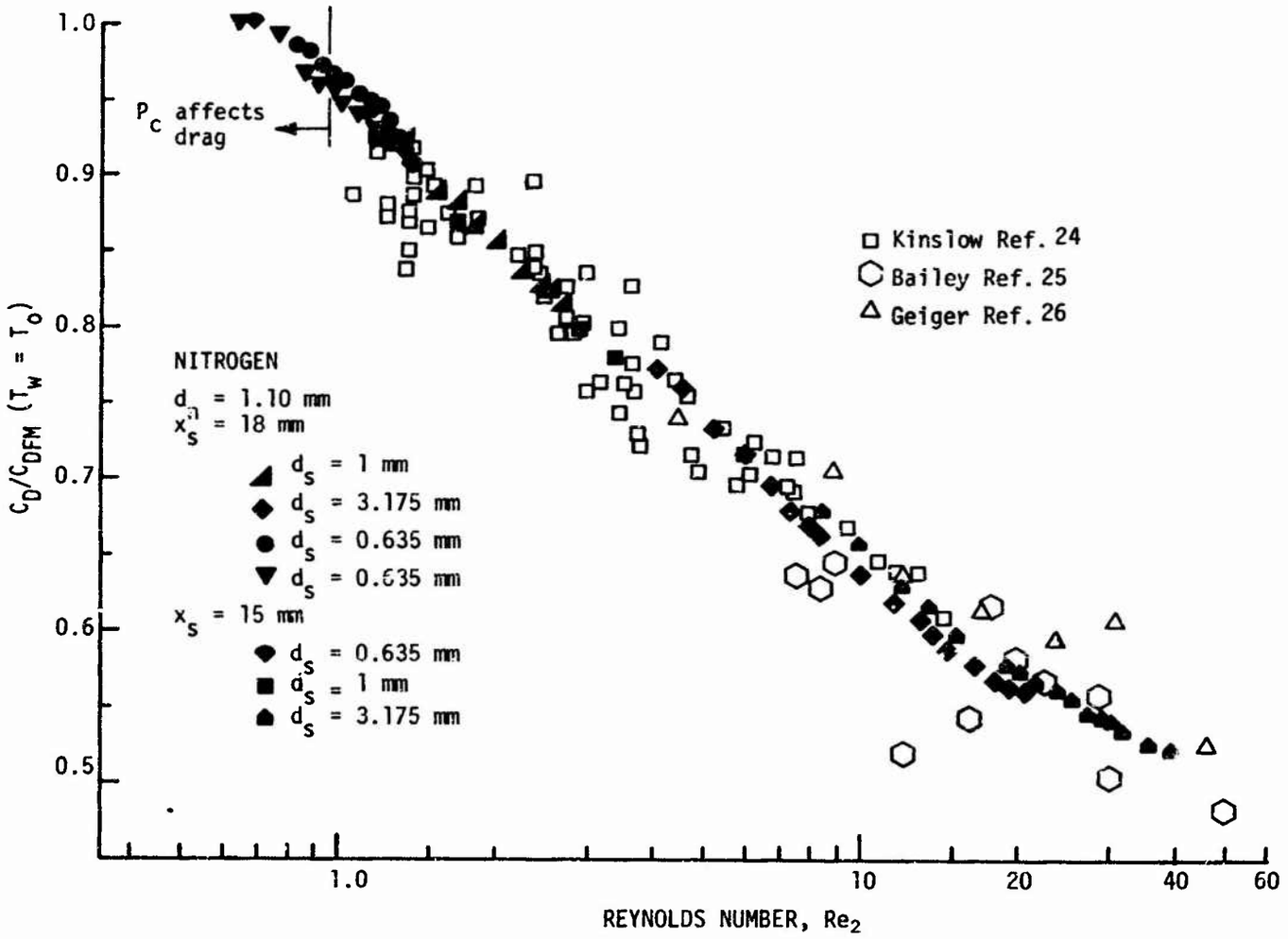

FIGURE 5.1 Normalized Drag Compared with Other Experimental Results (Flow Properties at Sphere Center Location)

the present data definitely tend toward the free molecular limit for stagnation wall temperatures in all tests.

In section IV-A mention was made of the fact that the drag coefficient tended to be higher when measured at smaller nozzle-sphere separations. The maximum difference observed was about 8-10% when comparing data at constant Knudsen number for 1/8 inch spheres at the minimum and maximum X_s/d_n values for nitrogen. The difference decreases with increasing Knudsen number to about 4% at near free molecular conditions. Any such discrepancy was considerably less when comparing any other stations and always less for argon.

B. Flow Properties Based on Sphere Stagnation Point

Although there is some slight Mach number effect (the free molecular drag coefficient is greater at lower Mach numbers), it does not appear to account for the difference observed. Even for the smallest distances at which tests were made the flow was hypersonic and very little Mach number effect is expected in this regime. A more reasonable assumption is that this difference is due to the axial gradients in the flow which cause a greater error for stations close to the nozzle and for larger spheres. The difference trend was eliminated for the 1/8 inch spheres by calculating the flow properties at the location of the stagnation point of the sphere instead of the center line location.

Some slight difference as a function of nozzle-sphere separation remained at higher Knudsen numbers (smaller sphere models) and this was attributed to the mass flow corrections discussed in Chapter II. The mass flow corrections were greater at the lower source pressures used to obtain high Knudsen numbers and even greater at the further reduced source pressures to produce the same Knudsen number at smaller nozzle-sphere separations. Therefore, if the data is slightly over-corrected by the effective nozzle size used, this effect would result in the difference observed. In any event, any consistent rise in the drag coefficient remaining with decreasing X_s/d_n is always less than 3% for data not influenced by the jet

flow field. This difference must be considered to be within the error of the results in view of the assumptions used in the data reduction.

Data reduced using the flow properties at the location of the sphere stagnation point are shown in Figure 5.2. Although this improved the internal agreement between the data taken at different sphere stations, the comparison with the free flight results is less impressive at higher Reynolds numbers. The disagreement is confined to the 1/8 inch spheres and, as has been mentioned, these are the least credible of the present data. Since the sphere size is approximately 3 times the nozzle diameter, the axial gradient influence is not negligible. It would seem, however, that the stagnation point is the more representative location from momentum transfer considerations.

The presentation of data in terms of properties at the front of the sphere indicates the same smooth increase toward the free molecular limit shown previously. These results are given in Figure 5.3 for nitrogen and Figure 5.4 (low X_s/d_n) and Figure 5.5 (high X_s/d_n) for argon as a function of free stream Knudsen number.

An additional comparison is made with the results of Smolderen, Wendt, and Naveau.[27] These results were taken with a sting-mounted sphere in a free jet using air at Mach 8.3 (X/d_n = 9.1). The comparison is shown in Figure 5.6. There is good agreement with the present nitrogen data taken at low nozzle-sphere separations and based on sphere center line properties. However, the data taken further downstream and/or based on stagnation point properties predict a later rise to the free molecular limit than Smolderen's results. (This can be seen in Figure 6.9 of the next section.) There may be some Mach number effect when comparing the data with those at large nozzle-sphere separations and the possibility of sting effects cannot be excluded. Also the calculation of Kn_∞ is questionable for the present results.

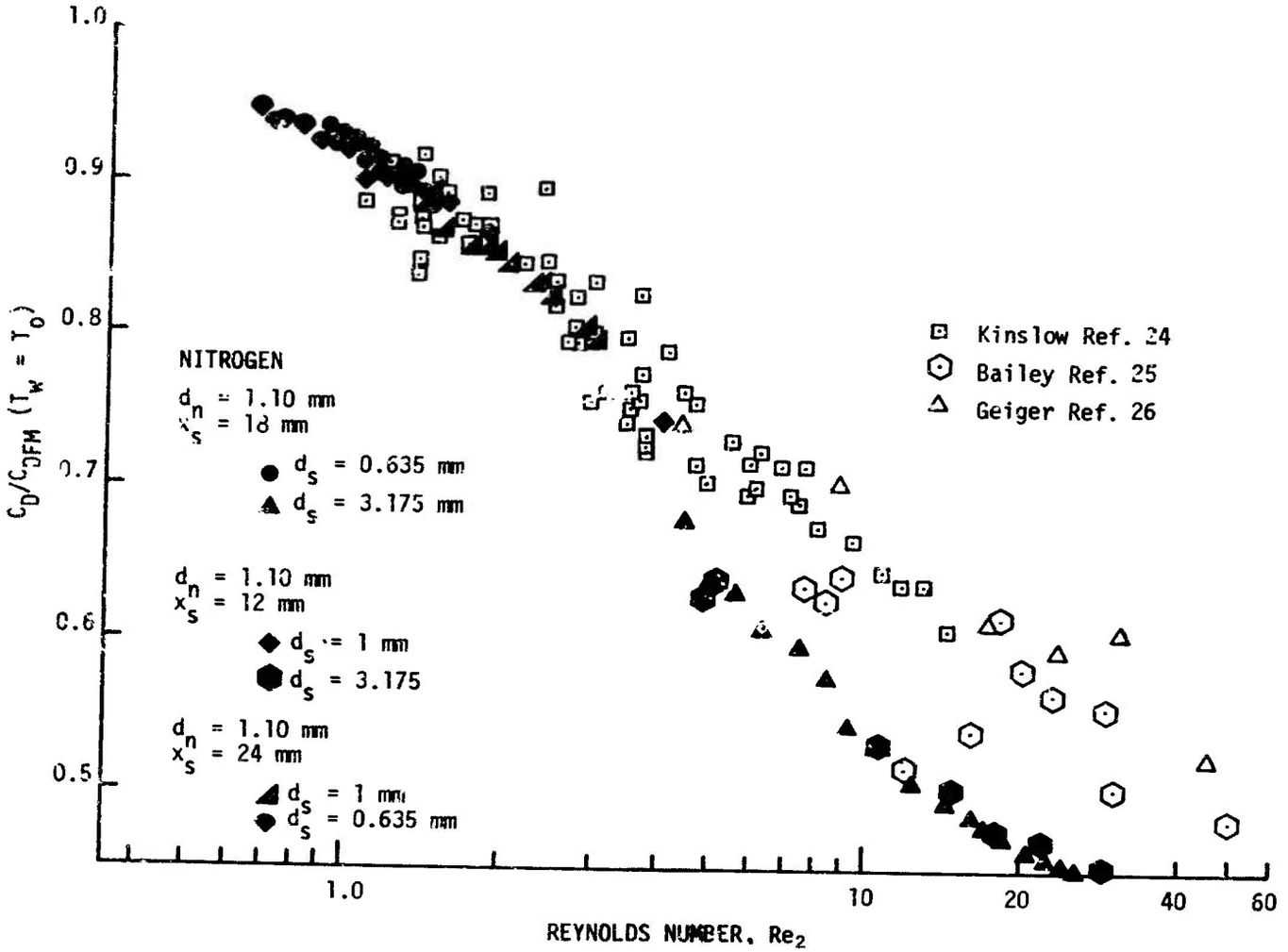

FIGURE 5.2 Normalized Drag Compared with Other Experimental Results (Flow Properties at Stagnation Point Location)

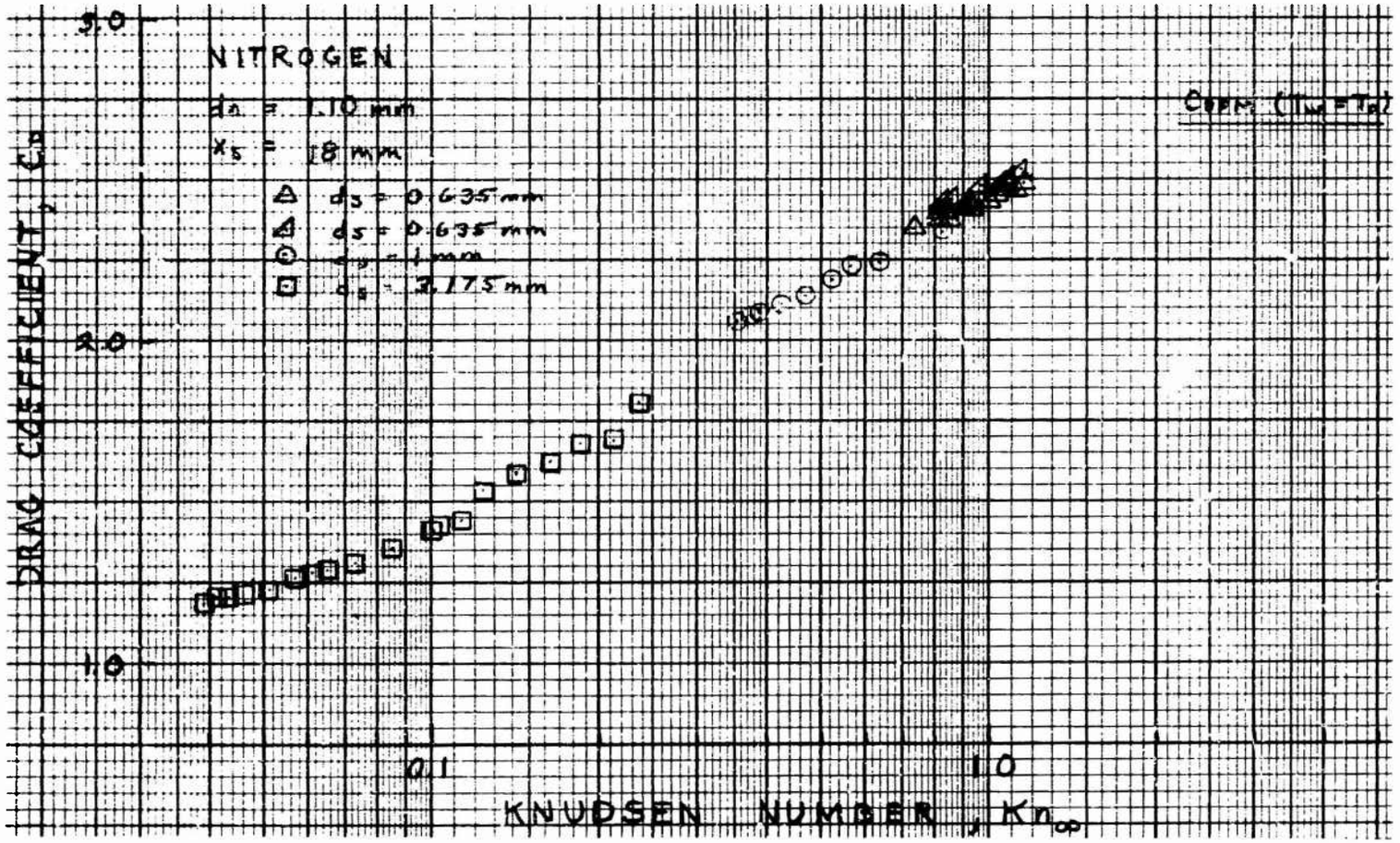

FIGURE 5.3 Sphere Drag vs. Knudsen No. (Int. x_s/d_n) for Nitrogen
(Flow Properties at Stagnation Point Location)

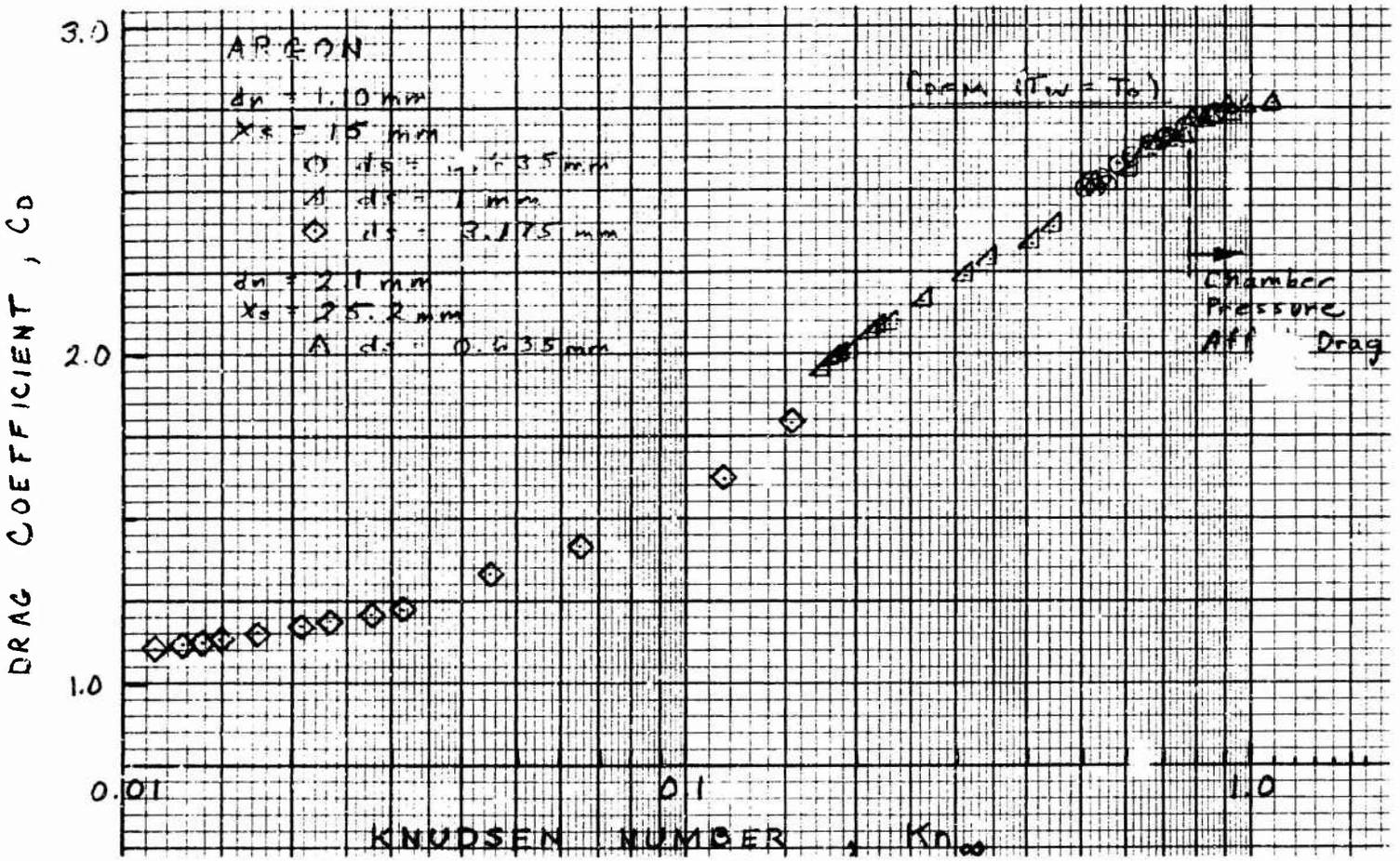

FIGURE 5.4 Sphere Drag vs. Knudsen No. (Low x_s/d_n) for Argon
(Flow Properties at Stagnation Point Location)

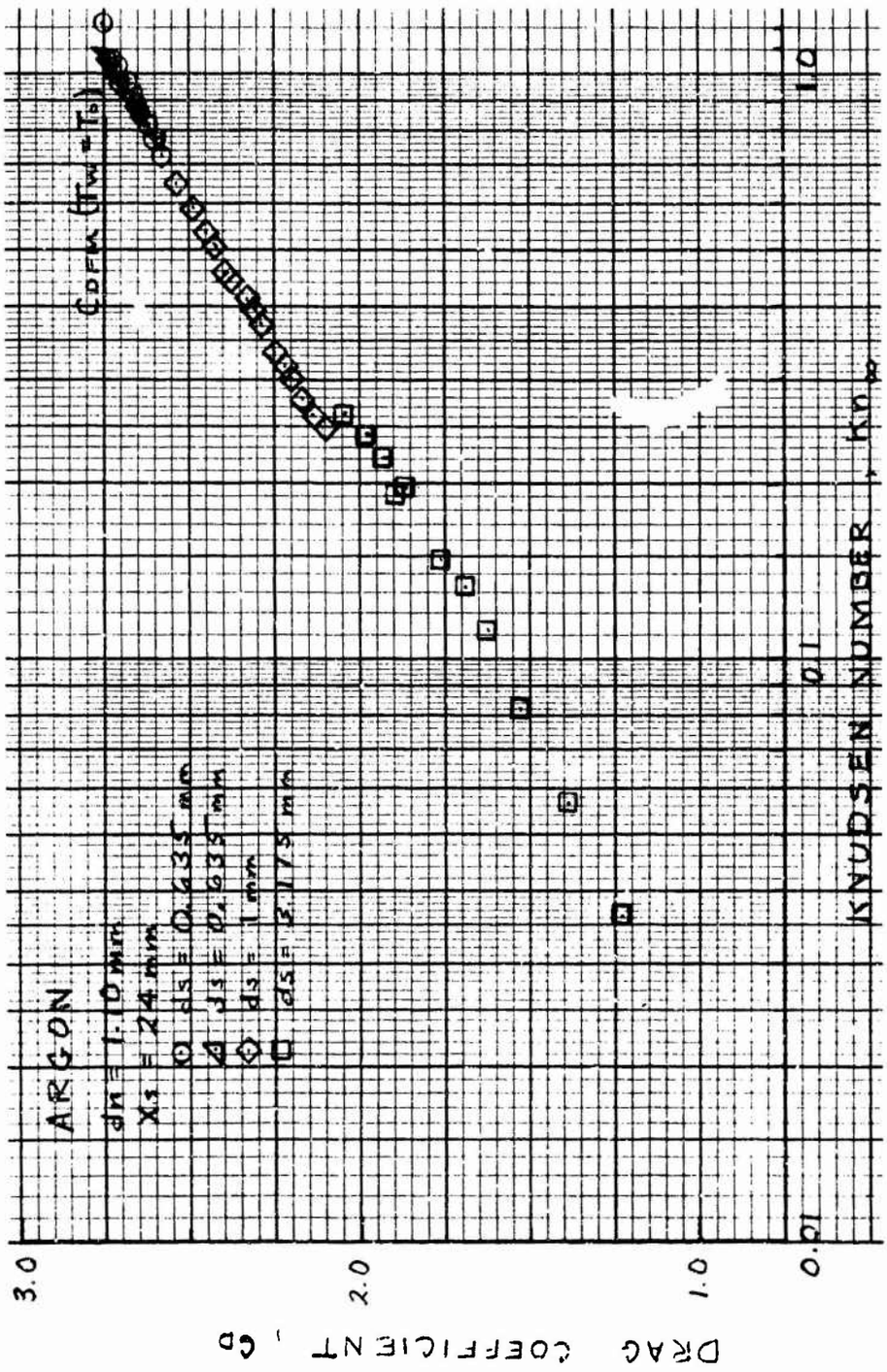

FIGURE 5.5 Sphere Drag vs. Knudsen No. (High x_s/d_n) for Argon
(Flow Properties at Stagnation Point Location)

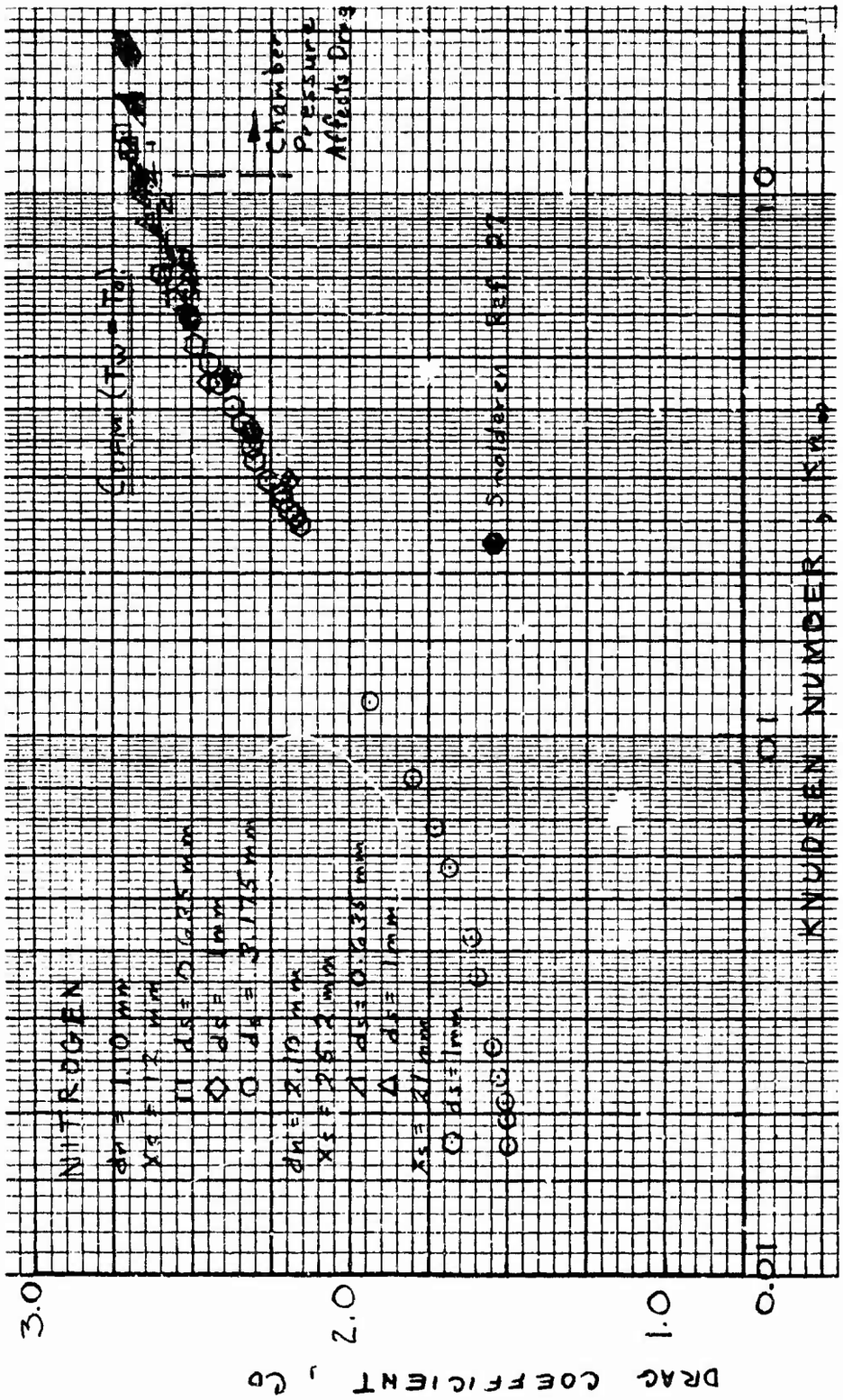

FIGURE 5.6 Sphere Drag vs. Knudsen No. (Low x_s/d_n) for Nitrogen
(Flow Properties at Sphere Center Line)

Sphere drag data has been taken by other investigators at low Mach numbers[†] in transition flow but those presented include the available hypersonic results. No comparison was available for argon.

[†]See for example references 28 and 29.

SECTION VI
COMPARISON WITH THEORETICAL MODELS

Comparison will be made with the results obtained by Willis[30,31] using the modified Krook model, the linearized Krook solution of Rose,[32] and the first collision results of Baker and Charwat.[33] Few theoretical computations for sphere drag in near free molecular flows are available and these are believed to represent those somewhat applicable to the present results.

A. Near Free Molecule Approaches

Willis[31] obtained a solution for sphere drag using the modified Krook model of Boltzmann's equation, assuming the body to be moving in a gas in thermal equilibrium at T_∞ with no ablation or absorption and the molecules leaving the body to have a Maxwellian distribution corresponding to some temperature, T_b. The analysis predicts a reduction of the free molecular drag in terms of the small parameter

$$\alpha = \delta n_\infty \frac{d_s}{2} \left(\frac{m}{2kT_b}\right)^{1/2} \tag{6.1}$$

where $1/\delta n_\infty$ is a relaxation time for translational energy and T_b is the temperature characterizing the reflected molecules. The constant δ was determined from

$$\delta = \frac{kT_\infty}{\mu_\infty} \quad . \tag{6.2}$$

If it is then assumed that the viscosity can be obtained from the Chapman-Enskog[34] relation

$$\mu = \rho\lambda\left(\frac{2kT}{\pi m}\right)^{1/2} \tag{6.3}$$

for hard sphere molecules, the parameter α can be written as

$$\alpha = \left(\frac{\sqrt{\pi}}{4}\right)\left(\frac{T_\infty}{T_b}\right)^{1/2} Kn_\infty . \tag{6.4}$$

Using these relations an analytic approximation to the computer solution for the drag of a sphere was given by Maslach, et al.[35] as

$$C_{DFM} - C_D = (0.165\ S_b + 1.44 - 1.13/S_b) \Big/ S_\infty Kn_\infty \ . \qquad (6.5)$$

The numerical results are for $S_b \geq 2$, diffuse reflection and large free stream Mach number. The parameter S_b is the body speed ratio defined as

$$S_b^2 = \frac{mV_\infty^2}{2kT_b} \qquad (6.6)$$

Here it will be assumed that $T_b = T_w = T_o$ and that

$$V_\infty^2 = \frac{2\gamma}{\gamma-1}\left(\frac{kT_o}{m}\right) \ . \qquad (6.7)$$

For the calculation, equation (6.5) was rearranged in the form

$$C_D = C_{DFM} - \left(\sqrt{\frac{T_\infty}{T_b}} \Big/ Kn_\infty\right)\left[0.165 + \frac{1.44}{S_b} - \frac{1.13}{S_b^2}\right] \qquad (6.8)$$

Using theoretical values of $\frac{T_\infty}{T_o} = \frac{T_\infty}{T_b}$ and $S_b = 1.871$ the results for nitrogen are shown in Figure 6.1 and 6.2. For the high X_s/d_n results shown in Figure 6.3 considerable liberty is taken in estimating the frozen value of T_∞ from Marrone[14] for the theoretical curves (to predict a maximum reduction from free molecular flow with the theory) and better agreement was obtained. Marrone's results are for rotational freezing and are higher than the freezing values for translation indicated by molecular beam studies.[36] Argon results are shown in Figure 6.4 for high X_s/d_n and $S_b = 1.581$. Figure 6.5 for argon at low X_s/d_n essentially repeats the data at high nozzle-sphere separations. The agreement of the data with the modified Krook model is good even though the condition

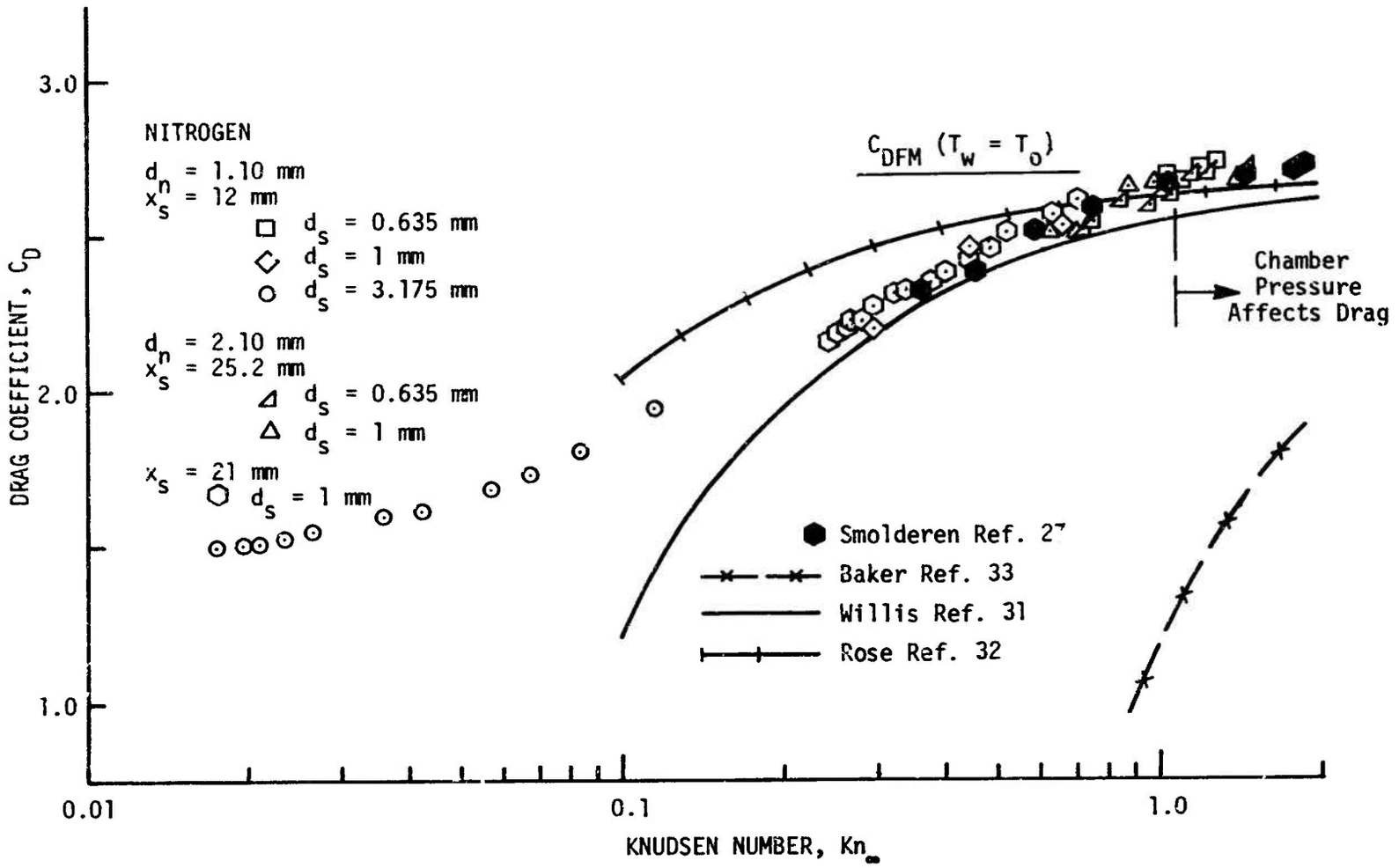

FIGURE 6.1 Sphere Drag vs. Free Stream Knudsen No. (Low x_s/d_n) for Nitrogen

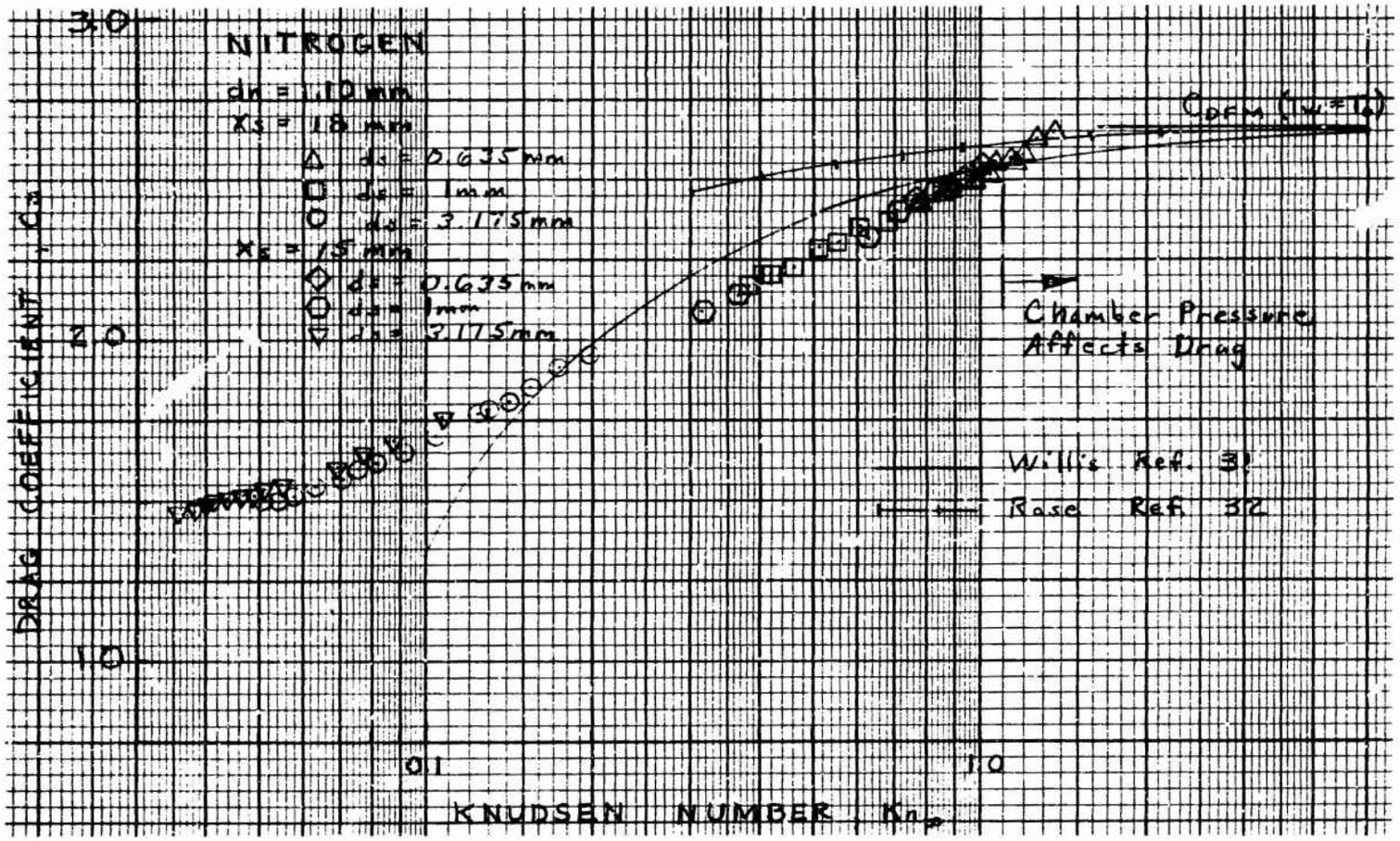

FIGURE 6.? Sphere Drag vs. Free Stream Knudsen No. (Int. x_s/d_n) for Nitrogen

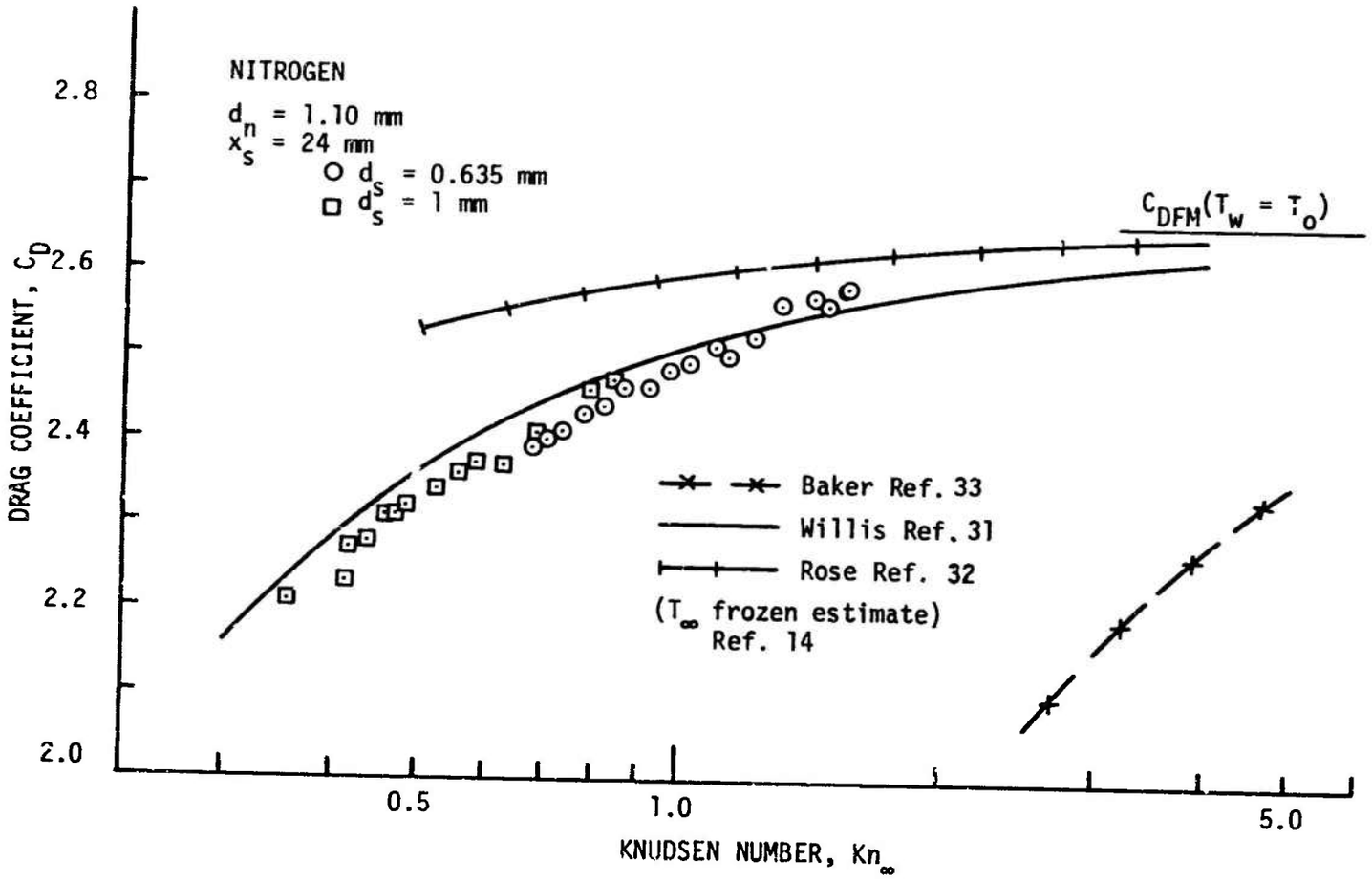

FIGURE 6.3 Sphere Drag vs. Free Stream Knudsen No. (High x_s/d_n) for Nitrogen

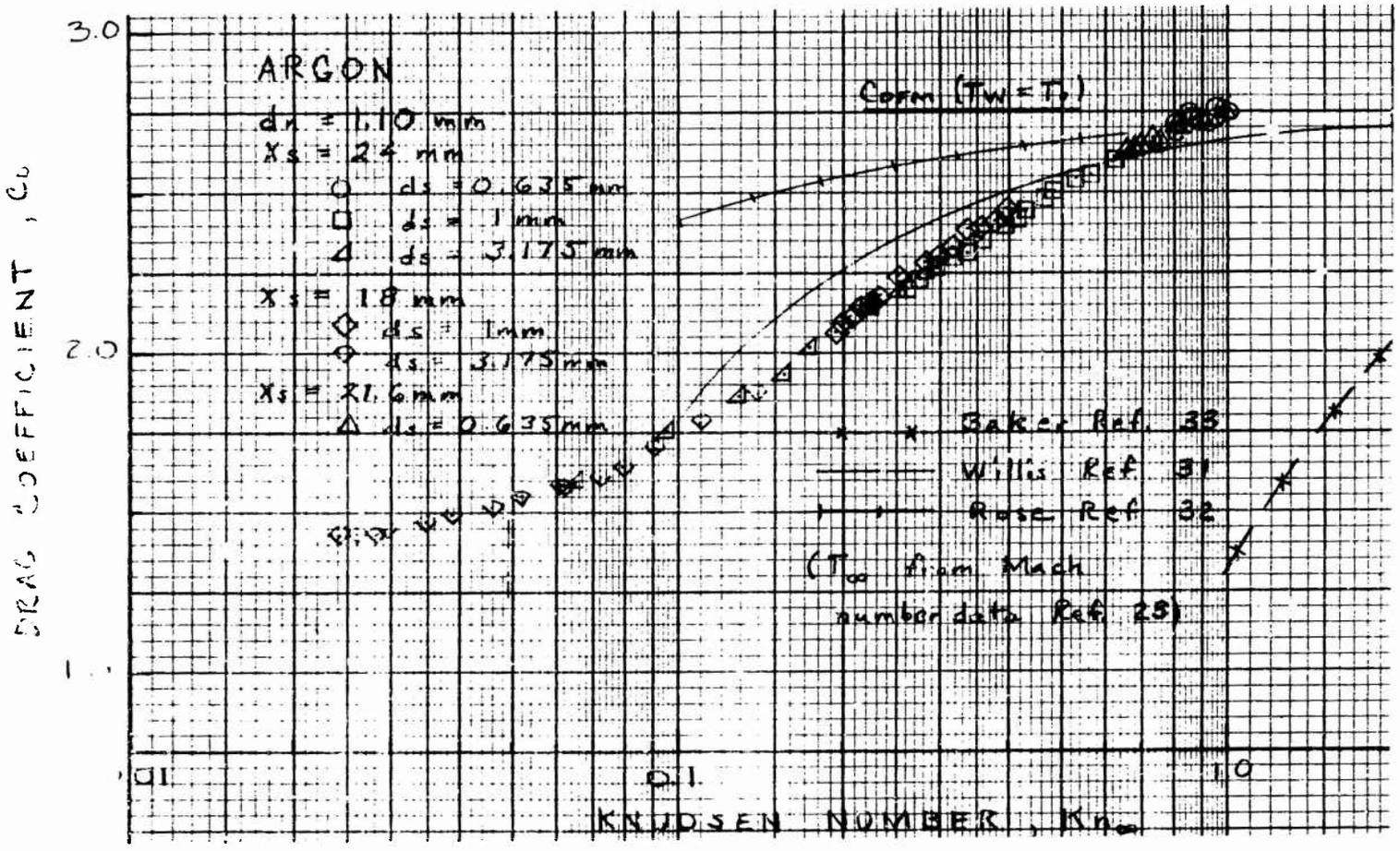

FIGURE 6.4 Sphere Drag vs. Free Stream Knudsen No. (High x_s/d_n) for Argon

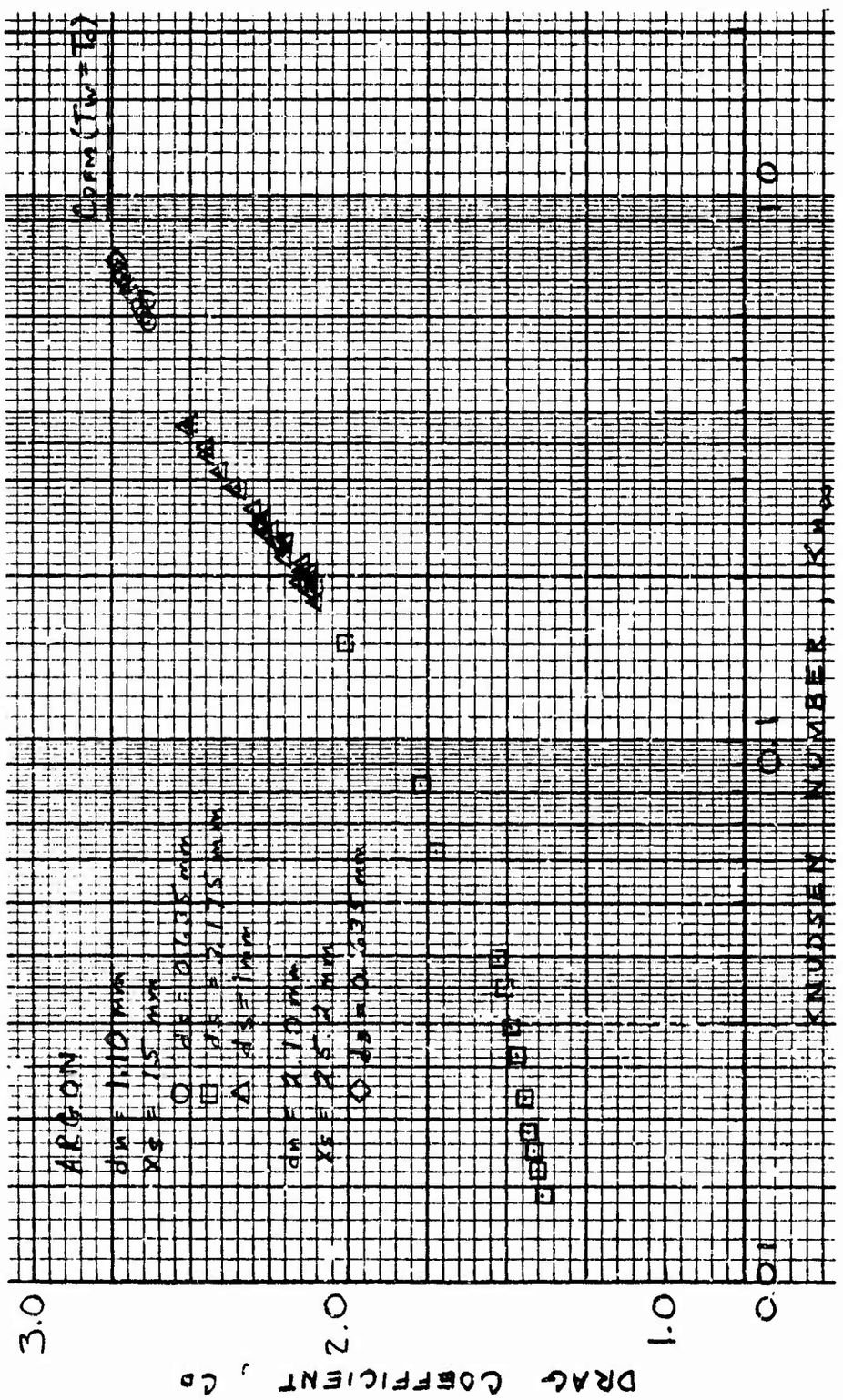

FIGURE 6.5 Sphere Drag vs. Free Stream Knudsen No. (Low x_s/d_n) for Argon

$S_b > 2$ is not fulfilled for the test results. The agreement is surprising when the assumptions made to calculate Kn_∞ are considered. The solution is only valid for small α and hence will fail at low Knudsen numbers. This is evident in Figure 6.2.

Baker and Charwat[33] obtained a first correction to the free molecular flow over a sphere by assuming that only first collisions between molecules are important. It was further postulated that the sphere was in a parallel and uniform beam of billiard-ball molecules, that reflected molecules have an average speed much less than free stream molecules, and that the mean free path of reflected molecules is independent of molecular velocity. The assumption of "slow" reflected molecules is violated in the present tests and would appear better for cold wall conditions. Willis[31] rearranged the results of Baker and Charwat in terms of the parameters used here and the resulting equation is

$$C_D = C_{DFM} - (0.24 S_b + 1.06) / Kn_\infty \ . \qquad (6.9)$$

The results were shown in Figures 6.1, 6.3 and 6.4 and are seen to be in serious disagreement with the data.

Rose[32] used the original Krook equation with the sphere represented by the addition of a point source term. The equation was linearized about the distribution function at infinity and solved using Fourier transform techniques. The assumptions used for the point source model and the linearization are diffuse reflection and

$$d_s << D << \lambda$$

and D is the observer position where the solution is valid. This restricts the solution to near free molecular flow. The first order solution obtained is

$$C_D = C_{DFM} - \frac{2}{Kn_R}\left[0.33\left(\frac{T_\infty}{T_b}\right)^{1/2} - 0.17/(\gamma)^{1/2}M\right] \qquad (6.10)$$

where Kn_R is a parameter used in the model. Rewriting equation (6.10) in terms of the variable used here[†]

$$C_D = C_{DFM} - \left(\sqrt{\frac{T_\infty}{T_b}}\Big/ Kn_\infty\right)\left(0.33 - \frac{0.12}{S_b}\right) \quad . \qquad (6.11)$$

The results are shown in Figures 6.1 through 6.4. The data are seen to depart quickly from agreement with these results.

Sherman et al.[37] postulated that for free jet testing the comparison with theory might best be made in terms of a parameter based on source conditions. This is indicated since such a parameter can be readily calculated and, with the body at about stagnation temperature, the important intermolecular collisions may be characterized by this temperature. The parameter suggested is

$$\alpha_o = \frac{\rho_\infty V_\infty d_s}{\mu_o}\left(\frac{T_o}{T_b}\right)^{1/2}\Big/ 4S_o \qquad (6.12)$$

where

$$S_o^2 = \frac{mV_\infty^2}{2kT_o} \quad . \qquad (6.13)$$

Here we will assume that $T_b = T_o$ and the parameter α_o is related to α given in equation (5.6) by

$$\alpha_o = \left(\frac{T_o}{T_\infty}\right)\left(\frac{\mu_\infty}{\mu_o}\right)\alpha \qquad (6.14)$$

Equations (6.8), (6.9) and (6.10) can be rewritten in terms of α and,

[†]Maslach et al.[35] listed these values. Slightly different constants result, depending on the relationship used to relate Kn_R and Kn_∞. However, the comparison with the data is qualitatively the same in all cases.

interpreting α as α_o the resulting equations are

$$C_D = C_{DFM} - \alpha_o \left[0.37 + \frac{3.32}{S_b} - \frac{2.57}{S_b^2} \right] \quad \text{(Willis)} \qquad (6.15)$$

$$C_D = C_{DFM} - \alpha_o \left[0.75 - \frac{0.26}{S_b} \right] \quad \text{(Rose)} \qquad (6.16)$$

$$C_D = C_{DFM} - \alpha_o \left[1 + \frac{4.36}{S_b} \right] \quad \text{(Baker and Charwat)} \qquad (6.17)$$

Data reduced using properties at the front of the sphere are compared with equations 6.15 - 6.17 in Figures 6.6 and 6.7 for nitrogen and Figure 6.8 for argon. Here we see a clear preference for agreement with the modified Krook solution.† The droop occurring at low values of α_o is due to data influenced by the jet structure. With nitrogen the sphere was assumed to be at stagnation temperature for the calculation of C_{DFM} and agreement is good. The argon data are in better agreement if the equilibrium temperature for an insulated sphere is used to calculate the free molecular value. In any event, the choice of C_{DFM} does not change the slope of the curve. The data shown in Figure 6.7 are taken further downstream and the boundary layer correction is less. This would appear to be the best data and good agreement is indicated with the linear dependence predicted by Willis.[31]

The data can be compared again in terms of the free stream variable Kn_∞. This comparison is shown in Figures 6.9 (low X_s/d_n) and 6.10 (high X_s/d_n). Although the agreement is slightly worse in terms of stagnation point properties, the modified Krook Model is clearly indicated to be the most applicable. Due to the fact that α_o can be calculated more accurately and would seem to better represent the collison process, preference is given to the linear comparison.

†Data based on center line properties show the same agreement with the tendency to be slightly below the prediction of Willis.

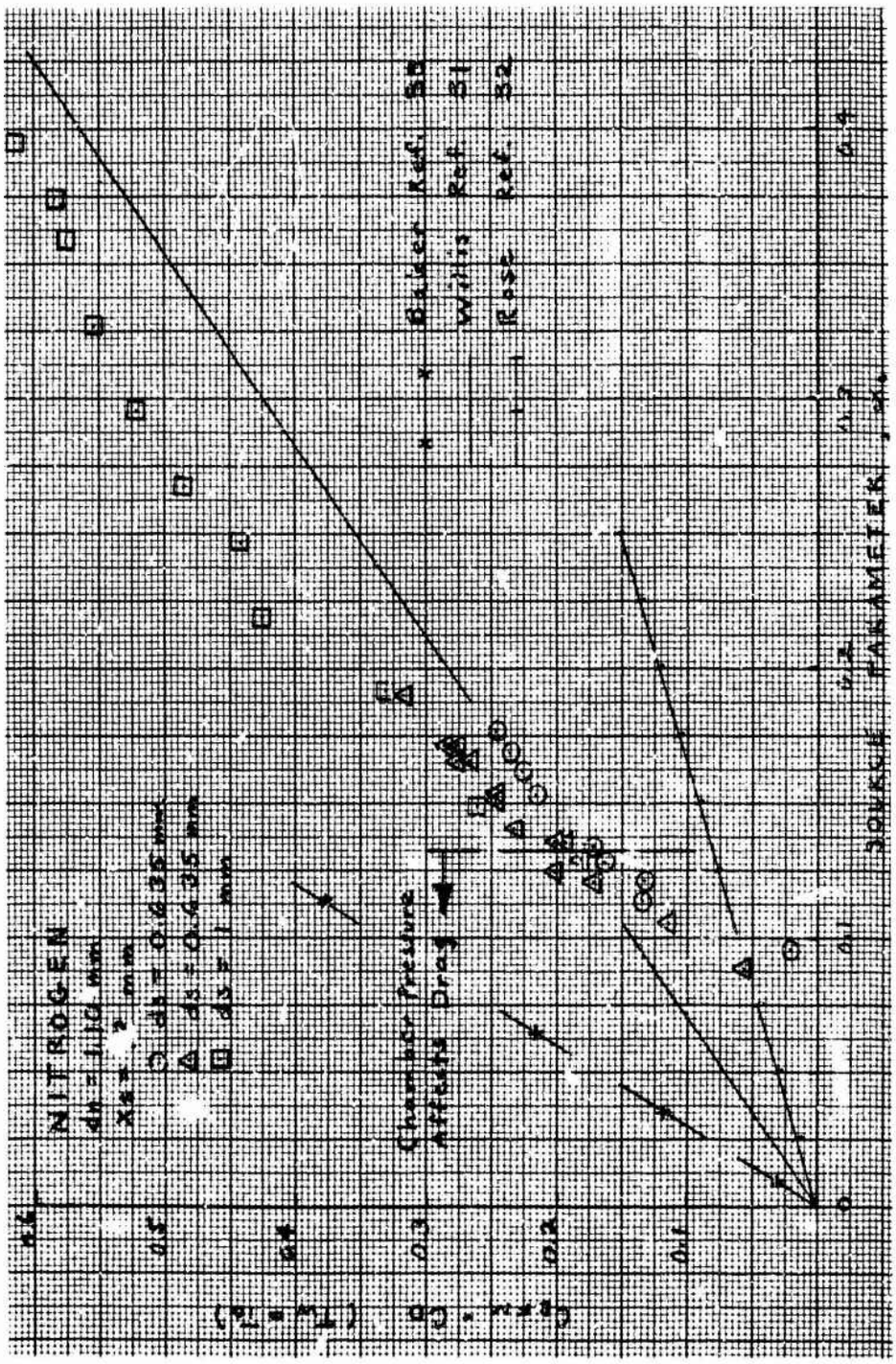

FIGURE 6.6 Comparison with Theory for Nitrogen (Stagnation Point Properties, Int. x_s/d_n) Based on Source Parameter

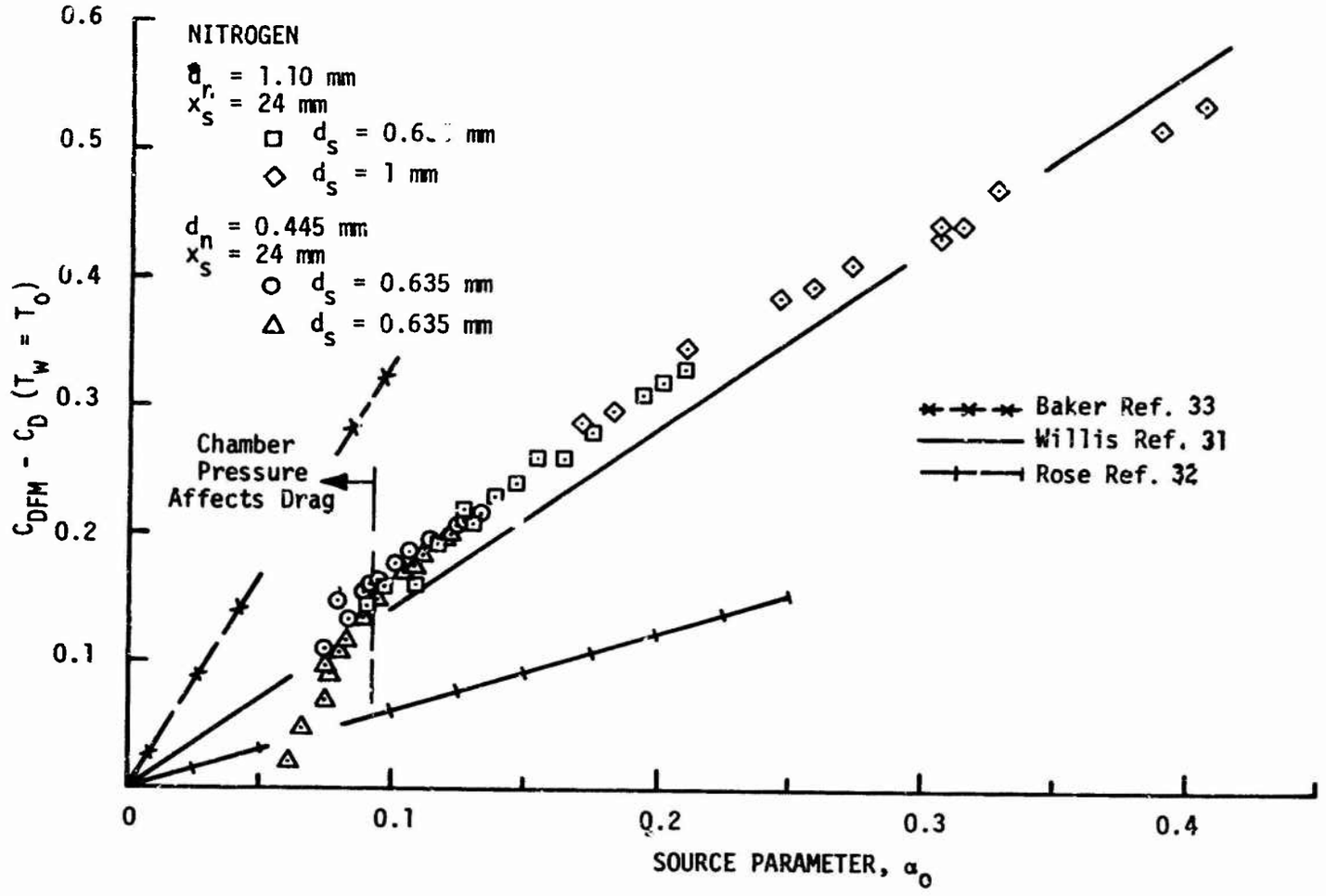

FIGURE 6.7 Comparison with Theory for Nitrogen (Stagnation Point Properties, High x_s/d_n) Based on Source Parameter

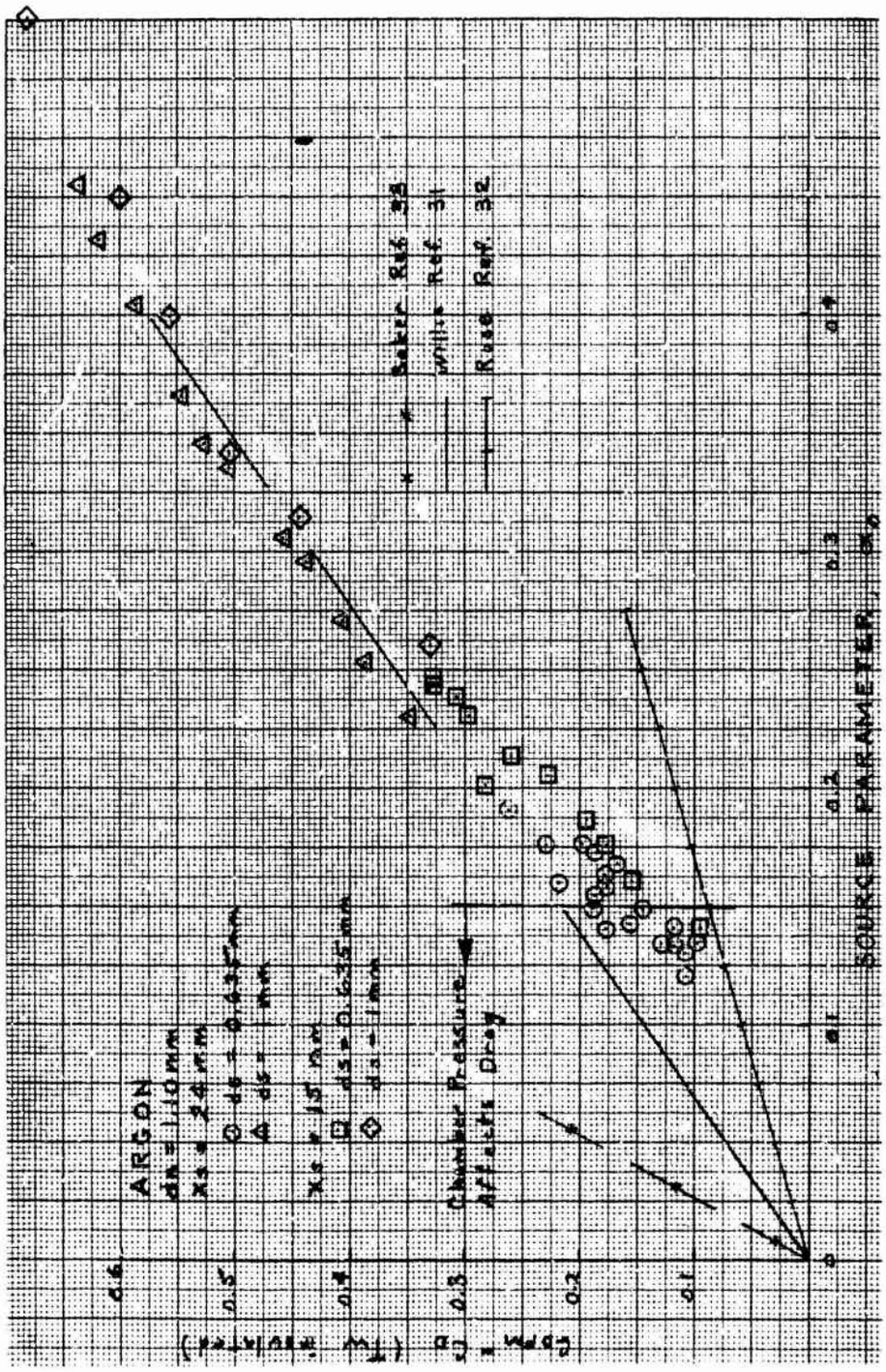

FIGURE 6.8 Comparison with Theory for Argon (Stagnation Point Properties) Based on Source Parameter

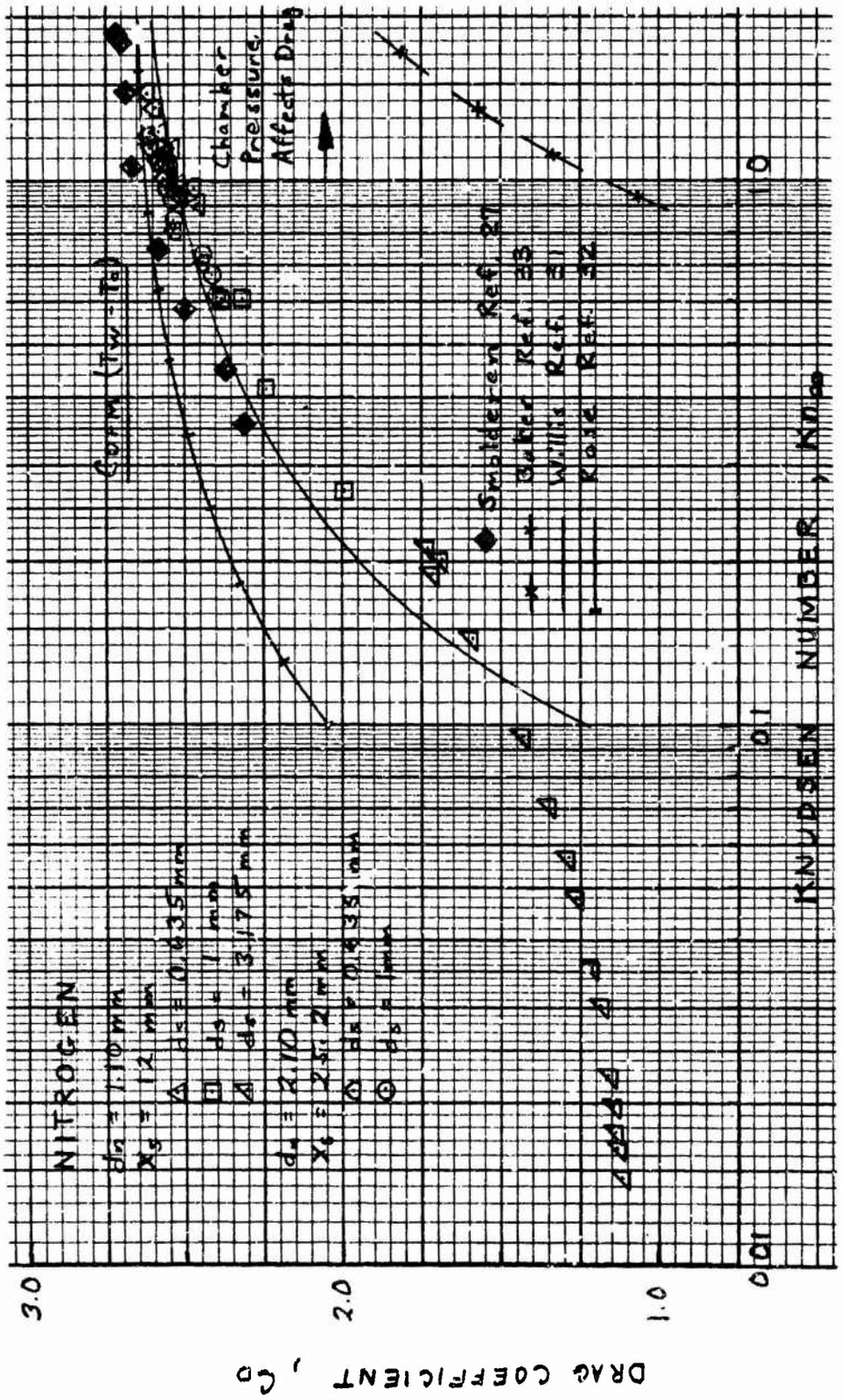

FIGURE 6.9 Comparison with Theory for Nitrogen (Stagnation Point Properties, Low x_s/d_n) Based on Knudsen No.

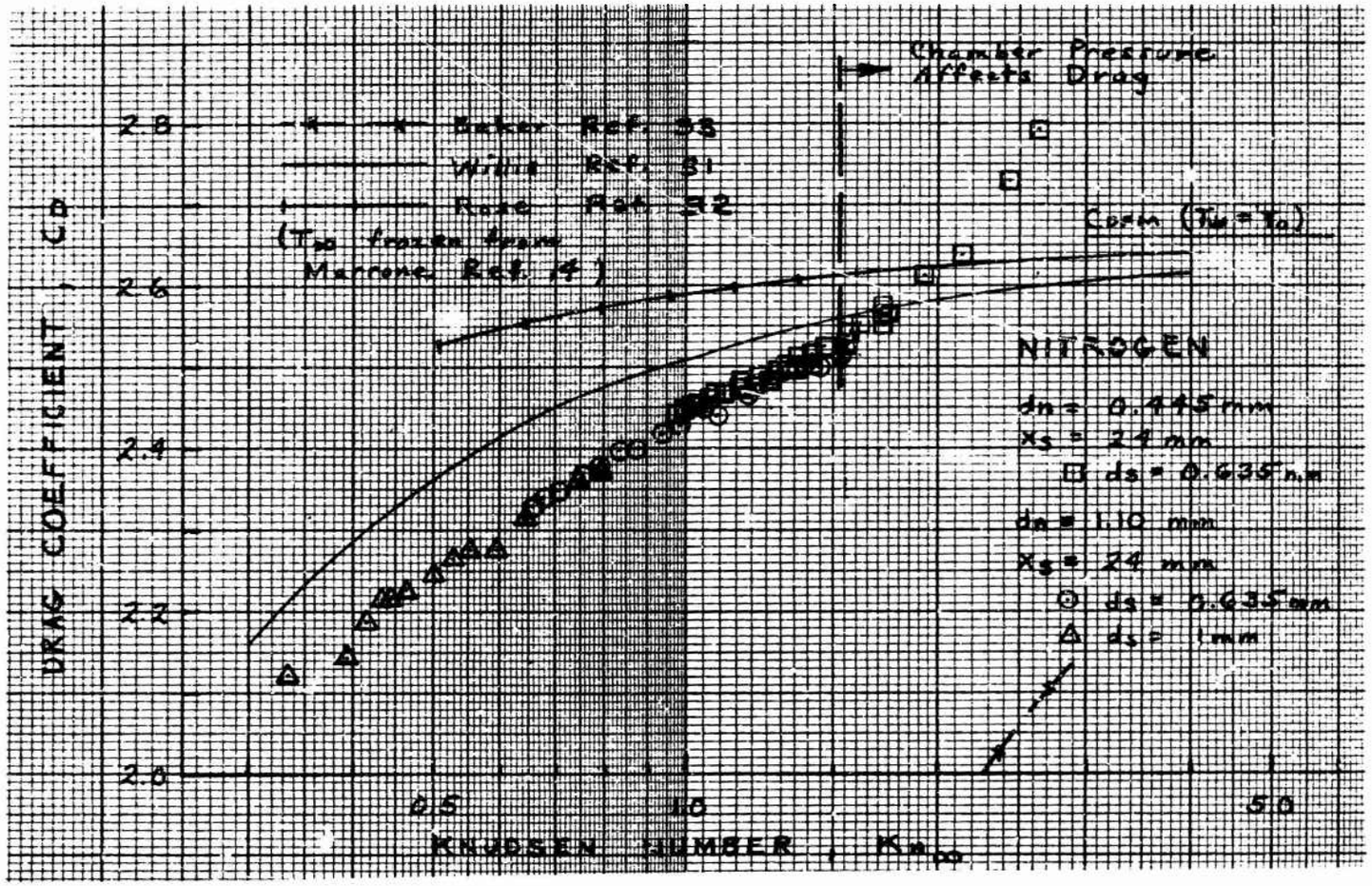

FIGURE 6.10 Comparison with Theory for Nitrogen (Stagnation Point Properties, High x_s/a_n) Based on Knudsen No.

B. Approaches from Continuum or Slip Flow

Davis and Flügge-Lotz[38] obtained a solution for departure from continuum flow by solving the boundary layer equations, including second order effects, for hypersonic flow over a blunt body. Only their numerical solution obtained for a sphere at Mach 10 with a wall to stagnation point ratio of 0.6 can be compared here. The results were only computed to first order in inverse $(Re_2)^{1/2}$ and are shown in Figures 6.11 and 6.12. The solution is for $\gamma = 1.4$ and viscosity proportional to the square root of the temperature. The value 0.89 is used for the pressure drag coefficient at high Reynolds number. Theoretical wall to free stream temperature ratios for the data are ~ 20 in Figure 6.11 and ~ 25 in Figure 6.12.† These compare to an assumed value of 12.6 for the model. The model must fail at low Reynolds numbers and is only shown to indicate that an extension of the data would be in general agreement as illustrated by Figure 6.12. The disagreement in Figure 6.11 can be removed by basing the flow properties on the stagnation point values, thereby lowering the high Reynolds number portion of the curve. The effect of this correction would be less in Figure 6.12. Figure 6.13 gives the argon data in terms of the familiar parameter of Reynolds number behind a normal shock. The behavior is similar to that for nitrogen.

Aroesty[28] suggested the same form for representing the drag coefficient in transition flow, i.e.,

$$C_D = C_{DI} = \frac{K_1}{\sqrt{Re_2}} + \frac{K_2}{Re_2} \qquad (6.18)$$

Kinslow and Potter[24] determined that K_2 was negative by fitting their data to this equation. The inviscid pressure drag term has been determined by Hodges[39] to be 0.92 and later by Bailey[25] to be 0.885. The value of 0.89 (in agreement with Davis[38]) was assumed here for nitrogen and the data for a

†Using the freezing value of rotational temperature from Marrone[14] and average values of $P_o d_n$ for the estimate, the ratios would be reduced to ~ 11 and ~ 15 respectively.

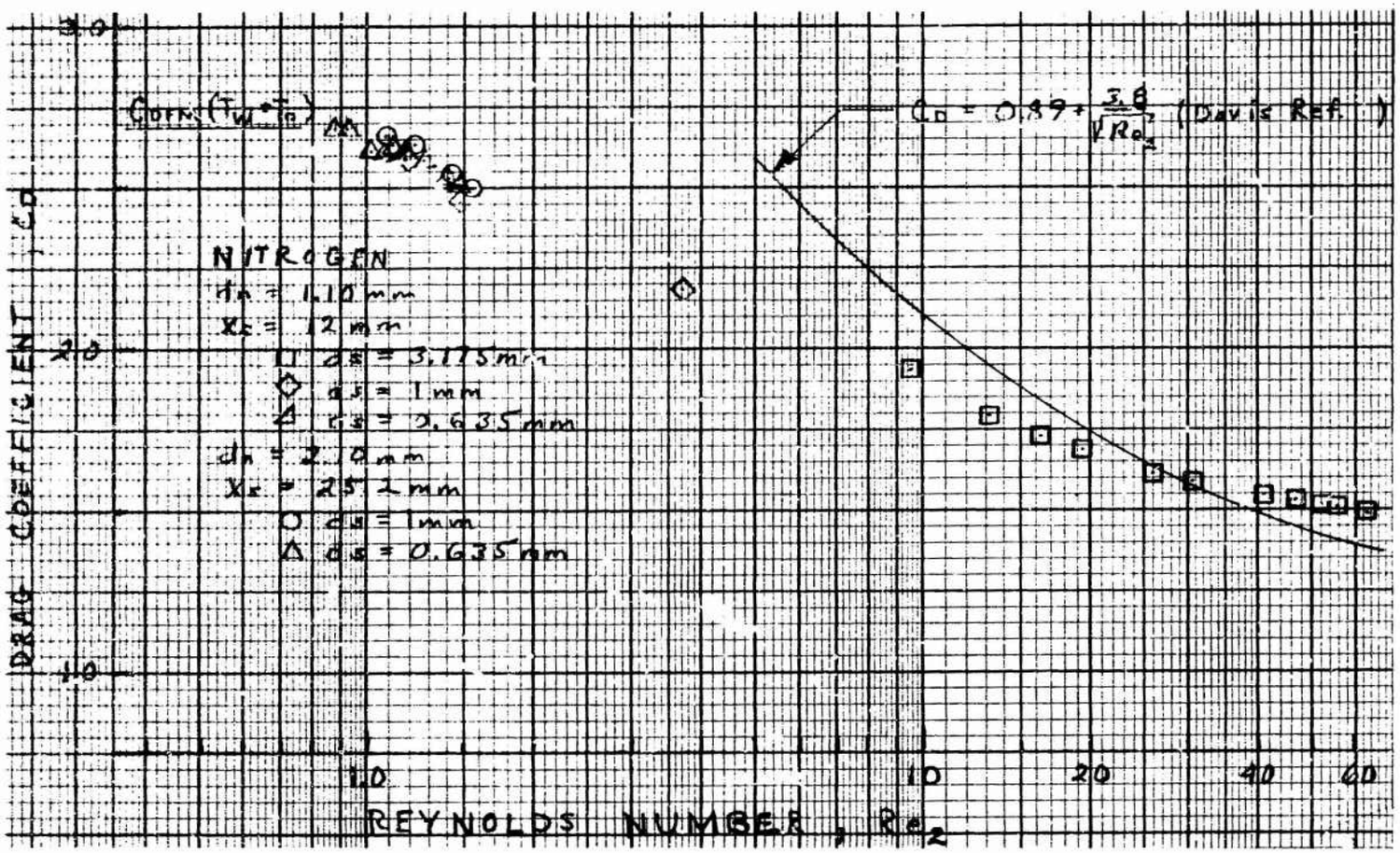

FIGURE 6.11 Sphere Drag vs. Reynolds No. Behind a Normal Shock (Low x_s/d_n) for Nitrogen

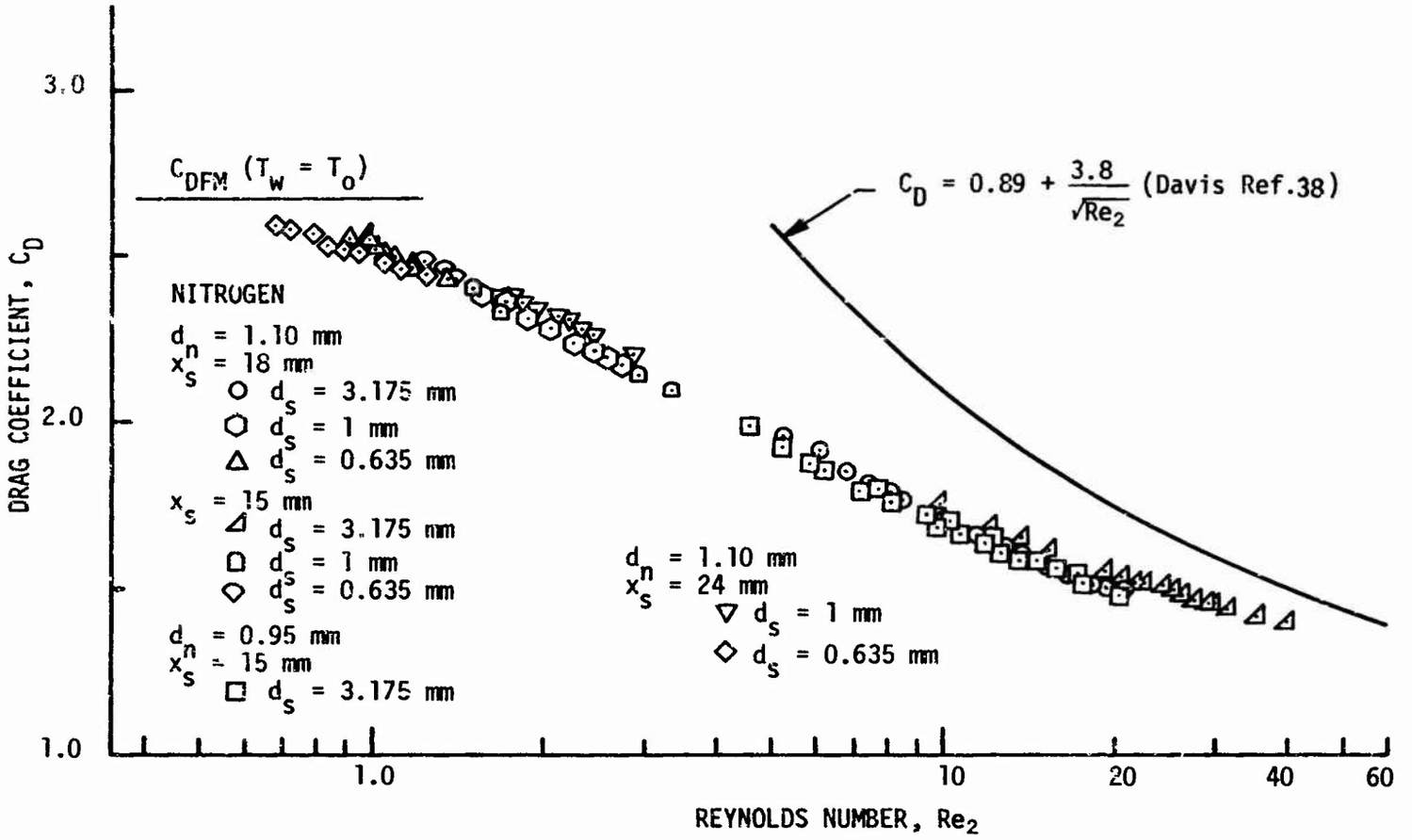

FIGURE 6.12 Sphere Drag vs. Reynolds No. Behind a Normal Shock (Int. x_s/d_n) for Nitrogen

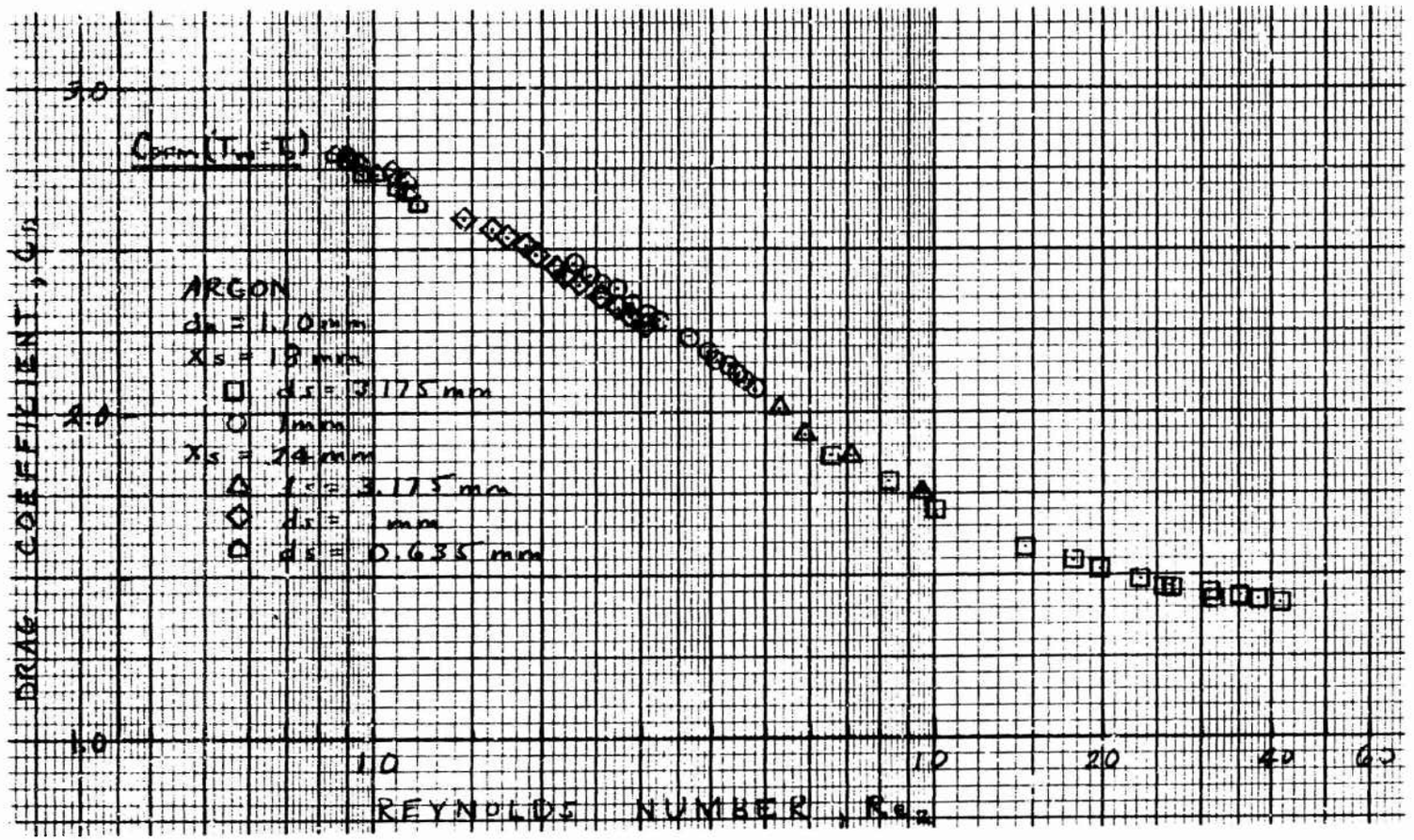

FIGURE 6.13 Sphere Drag vs. Reynolds No. Behind a Normal Shock (High x_s/d_n) for Argon

number of runs were fitted by least squares to equation (6.18). Typical results of the fittings are given in Table 2. In all cases K_2 is negative. The range of the values is evident as a function of nozzle sphere separation. Note that these constants are overly influenced by a large amount of data at very low Reynolds numbers and not sufficiently balanced by high Reynolds number data. The estimated value of 0.88 was used for C_{D1} with argon. The values of K_1 for nitrogen can be compared with the values of Davis[38] of 3.8 for $\frac{T_w}{T_\infty} = 12.6$ and 2.8 for $\frac{T_w}{T_\infty} = 4.2$ at Mach 10.

TABLE 2

CONSTANTS FOR DATA FIT

x_s/d_n	K_1	K_2	Standard Deviation σ
Nitrogen			
10.9	3.9	-2.1	$8.7(10^{-2})$
13.6	3.1	-1.5	$5.1(10^{-2})$
15.8	3.0	-1.4	$1.5(10^{-2})$
16.4	2.9	-1.3	$3.1(10^{-2})$
Argon			
13.6	3.6	-1.7	$3.8(10^{-2})$
16.4	3.1	-1.1	$3.6(10^{-2})$
21.8	3.1	-1.3	$2.5(10^{-2})$

SECTION VII

SUMMARY AND CONCLUSIONS

Extensive drag measurements have been made on spheres in the transition regime of gas dynamics. The data exhibit reduced scatter and improved repeatability compared with results previously available. The techniques employed have provided sting-free measurements while maintaining control over the model in a high velocity flow. A wide range of Knudsen numbers in near-free molecular flow has been investigated for both nitrogen and argon gases.

The findings of the investigation are:

1. The combination of the magnetic balance and free jet techniques represents a productive and comparatively inexpensive method for obtaining accurate drag data in high speed low-density flow.
2. General agreement has been demonstrated with the relatively limited data available for comparison.
3. The measurements verify the expected smooth increase in drag through the transition regime tending asymptotically to the free molecular limit (based on a diffuse thermally accommodated reflection model). There is no true tendency for any of the data to rise above this limit.
4. Good agreement is obtained over a reasonably wide range of flow conditions with the theoretical results of Willis using a modified Krook model.
5. Studies made with temperature variation of both the source gas and the sphere surface offer qualitative agreement with expectations; however, the experimental technique has not been sufficiently refined to allow quantitative comparison.

In addition, several observations can be made concerning the use of the free jet as a low density flow field.

1. Correlation parameters in terms of the source conditions and the local density are those most accurately determined in free jet testing and they appear to provide a successful correlation of the variation of drag coefficient in transition flow.
2. Drag measurements at large nozzle-sphere separations are the most repeatable, exhibit the least scatter, and require the least correction for effective nozzle size at the same local flow conditions. The latter is important since accurate mass flow measurements (used to correct the nozzle size) are difficult to obtain. However, attention must be paid to additional aspects such as temperature and Mach number "freezing" when testing at large nozzle-sphere separations.
3. The influence of the jet shock structure and background gas on the sphere drag may be successfully monitored by the chamber pressure variation tests.
4. For a fixed pumping system, low nozzle-sphere separations are best for testing at the near-continuum end of the transition regime, while near free molecular conditions are better simulated at large nozzle-sphere separations.
5. The discrepancy between data obtained at small nozzle-sphere separations and those obtained at large separations (occurring primarily for larger spheres in nitrogen) can be reduced by calculating the local flow properties at the leading stagnation point rather than at the sphere center.

BIBLIOGRAPHY

1. Schaaf, S. A. and P. L. Chambre', "Flow of Rarefied Gases," High Speed Aerodynamics and Jet Propulsion, Volume 3, Section H, Princeton University Press, 1958.

2. Tang, S., "Cylinder Drag in the Hypersonic Free Jets of a Rarefied Air Stream," UCB AS-64-3, 1964.

3. Ko, D. R., "Drag of a Two Dimensional Strip Normal to Hypersonic Near Free Molecular Flow," UCB AS-64-4, 1964.

4. Bier, K., and B. Schmidt, Z. Angew, Phys. 13, pp. 493-500, 1961.

5. Ashkenas, H. and F. S. Sherman, "The Structure and Utilization of Supersonic Free Jets in Low Density Wind Tunnels," Rarefied Gas Dynamics, Academic Press, Vol. 2, pp. 84-105, 1966.

6. Kuhlthau, A. R., "The Investigation of Low Density Drag Phenomena Utilizing Laboratory Techniques," Proc. Fourth U.S. Navy Symposium on Aeroballistics, November 12-14, 1957.

7. Jenkins, A. W. and H. M. Parker, "Electromagnetic Support Arrangement with Three Dimensional Control-I, Theoretical," J. Appl. Phys. Supplement No. 4, 2385, 1959.

8. Fosque, H. S. and G. H. Miller, "Electromagnetic Support Arrangement with Three Dimensional Control-II, Experimental," J. Appl. Phys., Supplement No. 4, 2045, 1959.

9. Parker, H. M. and A. R. Kuhlthau, "A Magnetic Wind Tunnel Balance," University of Virginia, Research Laboratories for the Engineering Sciences, Report AST-4320-150-64U (AFOSR-64-0567), February, 1964.

10. Dancy, W. H., Jr., and W. R. Towler, "Three Dimensional Magnetically Supported Wind Tunnel Balance," Rev. Sci. Inst., 37, 1643-8, December 1966.

11. Parker, H. M., "Principles, Typical Configurations and Characteristics of the University of Virginia Magnetic Balance," Summary of ARL Symposium on Magnetic Wind Tunnel Model Suspension and Balance Systems, ARL 66-1135, 137-158, July 1966.

12. Phillips, W. M., "Drag Studies with a Magnetically Supported Sphere," unpublished DSc. Dissertation, University of Virginia, June 1968.

13. Owen, P. L. and C. K. Thornhill, "The Flow in an Axially-Symmetric Supersonic Jet from a Nearly-Sonic Orifice into a Vacuum," Aero. Res. Council Reports and Memoranda 2616, Great Britain, September 1948.

14. Marrone, P. V., "Temperature and Density Measurements in Free Jets and Shock Waves," Physics of Fluids, Vol. 10, No. 3, 521-538, March 1967.

15. Muntz, E. P., "Measurements of Anisotropic Velocity Distribution Functions in Rapid Radial Expansions," Rarefied Gas Dynamics, Vol. II, pp. 1257-1286, Academic Press, 1967.

16. Hirschfelder, J. O., C. F. Curtis, and R. B. Bird, Molecular Theory of Gases and Liquids, John Wiley, New York, 1954.

17. Reis, V. H., "Free Expansion of Pure and Mixed Gases from Small Nozzles," Princeton Report FLD-7, May 1962.

18. Lefkowitz, "A Study of Rotational Relaxation in a Low Density Hypersonic Free Jet by Means of Impact Pressure Measurements," UCLA Rept. 67-27, July 1967.

19. Bier, K. and O. Hagena, "Influence of Shock Waves on the Generation of High-Intensity Molecular Beams by Nozzles," Rarefied Gas Dynamics, Vol. I, pp. 478-496, Academic Press, New York, 1963.

20. Gregorek, G. M. and R. G. Luce, "Axisymmetric and Planar Free Jets for Hypersonic Low Density Test Facilities," ARL 66-0068, April 1966.

21. Christ, S., P. M. Sherman and D. R. Glass, "Study of Highly Underexpanded Sonic Jet," AIAA Journal, Vol. 4, No. 1, p. 68, January 1966.

22. Patterson, G. N., "Mechanics of Rarefied Gases and Plasmas," UTIA Review No. 18, March 1962.

23. Scott, John E., Jr. and J. A. Phipps, "Translational Freezing in Freely Expanding Jets," Rarefied Gas Dynamics, Vol. 2, pp. 1337-1352, Academic Press, New York, 1967.

24. Kinslow, M. and J. L. Potter, "The Drag of Spheres in Rarefied Hypervelocity Flow," AEDC-TDR-62-205, December 1962.

25. Bailey, A. B., "High Speed Drag in the Transition Flow Regime in an Aeroballistic Range," Rarefied Gas Dynamics, Vol. II, pp. 1127-1143, 1967.

26. Geiger, R. E., "Some Sphere Drag Measurements in Low-Density Shock Tunnel Flows," GER63SD23, July 1963.

27. Smolderen, J. J., J. F. Wendt and J. Naveau, "The Meausrement of Drag Forces in Low Density Flows," Presented at IAF, Belgrade, September 1967.

28. Aroesty, J., "Sphere Drag in Low Density Supersonic Flow," Univ. of California, Report No. HE-150-192, January 1962.

29. Sreekanth, A. K., "Drag Measurements on Circular Cylinders and Spheres in the Transition Regime at a Mach Number of Two," UTIA Report No. 74, April 1961.

30. Willis, D. R., "On the Flow of Gases under Nearly-Free Molecular Conditions," Princeton Engr. Report. No. 442 (AFOSR TN 58-1093), December 1958.

31. Willis, D. R., "Methods of Analysis of Nearly-Free Molecular Flow for a Satellite or Other Space Vehicle," T.i.S. Report R60SD399, August 1960.

32. Rose, M., "Drag on an Object in Nearly-Free Milecular Fow," The Physics of Fluids, Vol. 7, No. 8, pp. 1262-1269, August 1964 (See also NYO-10427).

33. Baker, R. M. L., Jr. and A. F. Charwat, "Transitional Correction to the Drag of a Sphere in Free Molecular Flow," The Physics of Fluids, Vol. 1, No. 2, pp. 73-81, March-April 1958.

34. Chapman, S. and T. G. Cowling, The Mathematical Theory of Non-uniform Gases, Cambridge University Press, 1961.

35. Maslach, G. J., D. R. Willis, S. Tang and D. Ko, "Recent Experimental and Theoretical Extensions of Nearly Free Molecular Flow," Rarefied Gas Dynamics, Vol. I, Section 4, pp. 433-442, Academic Press, New York, 1965.

36. Hagena, O. F., J. E. Scott, Jr. and A. K. Varma, "Design and Performance of an Aerodynamic Molecular Beam and Beam Detection System," RLES Report No. AST-4038-103-67U, University of Virginia, June 1967.

37. Sherman, F. S., D. R. Willis and G. J. Maslach, "Nearly-Free Molecular Flow: A Comparison of Theory and Experiment," UCB Report No. AS-64-16, October 1964.

38. Davis, R. T. and I. Flügge-Lotz, "Second-Order Boundary-Layer Effects in Hypersonic Flow Past Axisymmetric Blunt Bodies," Journal of Fluid Mechanics, Vol. 20, Part 4, pp. 593-623, 1964.

39. Hodges, A. J., "The Drag Coefficient of Very High Velocity Spheres," Journal of the Aeronautical Sciences, Vol. 24, No. 10, pp. 755-758, October 1957.

40. Wang, C. J., J. B. Peterson and R. Anderson, "Gas Flow Tables," TRW GM-TR-154, March 1958.

41. Liepmann, H. W. and A. Roshko, Elements of Gasdynamics, Wiley, New York, 1957.

42. Dushman, S., Scientific Foundations of Vacuum Technique, Wiley, New York, 1965.

UNCLASSIFIED

Security Classification

DOCUMENT CONTROL DATA - R & D

(Security classification of title, body of abstract and indexing annotation must be entered when the overall report is classified)

1. ORIGINATING ACTIVITY *(Corporate author)*
Research Laboratories for the Engineering Sciences
University of Virginia
Charlottesville, Virginia 22901

2a. REPORT SECURITY CLASSIFICATION

2b. GROUP

3. REPORT TITLE
THE MEASUREMENT OF SPHERE DRAG IN A RAREFIED GAS USING A MAGNETIC WIND TUNNEL BALANCE

4. DESCRIPTIVE NOTES *(Type of report and inclusive dates)*
Scientific Final

5. AUTHOR(S) *(First name, middle initial, last name)*
W. M. PHILLIPS
A. G. KEEL, Jr.
A. R. KUHLTHAU

6. REPORT DATE	7a. TOTAL NO. OF PAGES	7b. NO. OF REFS
April 1970	79	42

8a. CONTRACT OR GRANT NO.	9a. ORIGINATOR'S REPORT NUMBER(S)
AF-AFOSR-1046-67	AEEP-3435-115-70U
b. PROJECT NO. 9783-01	
c. 61102F	9b. OTHER REPORT NO(S) *(Any other numbers that may be assigned this report)* AFOSR 70-1588TR
d. 681307	

10. DISTRIBUTION STATEMENT
1. This document has been approved for public release and sale; its distribution is unlimited.

11. SUPPLEMENTARY NOTES	12. SPONSORING MILITARY ACTIVITY
TECH, OTHER	AF Office of Scientific Research (SREM) 1400 Wilson Boulevard Arlington, Virginia 22209

13. ABSTRACT

Drag measurements on spheres in high speed transition regime flow are presented. The spheres are suspended electromagnetically in the low density flow field from a jet expanding freely from a small sonic nozzle into a vacuum. This arrangement provides sting-free measurements under hypersonic conditions. The current in the control coil of the electromagnetic balance is proportional to the applied force and provides a sensitive determination of the small forces encountered.

Data were taken using nitrogen and argon gases. A number of nozzle and sphere sizes were employed covering a Knudsen number range of 0.05 to 5. The results exhibit a smooth increase in the transition regime drag coefficient toward the free molecular limit for diffuse reflection and complete thermal accommodation.

Comparison is made with the available experimental results of other techniques. Improved repeatability and an extension of range of flow parameters is obtained with the present methods. The data are compared with current near-free molecular flow theories and the modified Krook solution of Willis is found to give the best agreement with the experimental results.

DD FORM 1 NOV 68 1473

UNCLASSIFIED

Security Classification

14. KEY WORDS	LINK A		LINK B		LINK C	
	ROLE	WT	ROLE	WT	ROLE	WT
sphere drag						
aerodynamic drag						
rarefied gas dynamics						
low density flow						
electromagnetic suspension						
magnetic wind tunnel balance						
free jet wind tunnels						